Machining Feature Based Geometric Modeling of Twist Drills

Jiang Zhu

A Thesis

in

The Department

of

Mechanical & Industrial Engineering

Presented in Partial Fulfillment of the Requirements

for the Degree of Master of Applied Science (Mechanical Engineering) at

Concordia University

Montreal, Quebec, Canada

August 2011

CONCORDIA UNIVERSITY

School of Graduate Studies

This is to certify that the thesis prepared

By: Jiang Zhu

Entitled: Machining Feature-based Geometric Modeling of Twist Drills

and submitted in partial fulfillment of the requirements for the degree of

Master of Applied Science

complies with the regulations of the University and meets the accepted standards with respect to originality and quality.

Signed by the final examining committee:

_____Dr. A. K. W. AHMED_____ Chair

_____Dr. A. AGUNDUZ_____ Examiner

_____Dr. W. TIAN_____ Examiner

_____Dr. C. Z. CHEN_____ Supervisor

Approved by _____Dr. MARTIN D. PUGH_____
Chair of Department or Graduate Program Director

_____Dr. ROBIN DREW_____
Dean of Faculty

Date ____SEPTEMBER 15, 2011_____

Abstract

Machining Feature Based Geometric Modeling of Twist Drills

Jiang Zhu

To pursue high accuracy, efficiency and reliability in the machining industry, high quality cutting tools play an important role. It is always in high demand in industry for new cutting tools in order to achieve better cutting performance and lower machining costs. To develop a new tool, a new approach is first to establish the accurate solid model of the tool, second to predict the tool performance in machining in order to optimize the tool, and third to grind the tool on a 5-axis grinding machine. To ensure the geometric model of a twist drill in good agreement with the machined one, a new approach to geometric modeling of the twist drill based on parametric machining features is proposed. In this work, the solid model of a twist drill includes four machining features, such as the flutes, the first flank, the drill split (gash), and the land. These features are parameterized based on the grinding wheel geometry and the 5-axis grinding wheel path. The effective grinding edge is calculated, and the geometric model is established. This approach is implemented in the CATIA V5 R20 to build the solid model of the twist drill. This model is genuine in terms of the actual machined twist drills. Therefore, it is essential to predict its machining performance of the actual cutters in machining simulation.

Acknowledgements

I wish to express sincere gratitude to my supervisor, Dr. Chevy Chen, for getting the thesis started in the positive and right direction. It was Dr. Chen who instilled the desire in my heart to develop an accurate model of twist drill of such level, which is genuine in accordance to the actually machined drill. I also wish to extend a measure of gratitude to my fellows, Shuangxi Xie, Chun Du, Maqsood Khan, and Muhammad Wasif, in CAD/CAM lab office. These gentlemen were tireless of answering my questions. When I encountered a problem, they helped me and inspired me.

Especially, I would like to give my special thanks to my wife and my two kids whose love enabled me to complete this work.

Table of Contents

List of Figures

List of Tables

Chapter 1 Introduction

Of all machining processes, drilling is very important because nearly 25% of the metal cutting processes are drilling operations and approximately 40% of workpiece materials are removed by drills [1]. Throughout the past century, twist drills have been drastically improved and have played an important role in the metal cutting industry. Up to now, more than 200 types of twist drill points have been shown in the literature and market. Figure 1-1 shows a standard twist drill, and Figures 1-2 to 1-8 show some common drill points in the market.

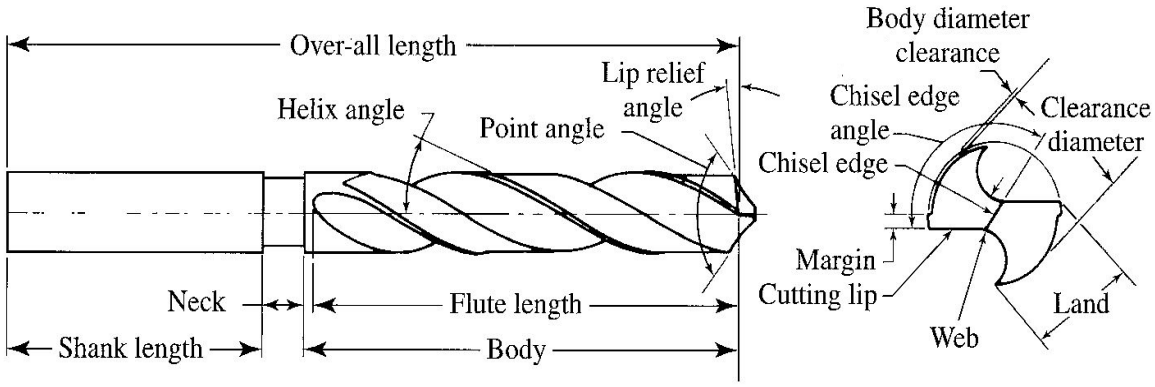

Figure 1-1 Standard geometry of a two flute twist drill [1]

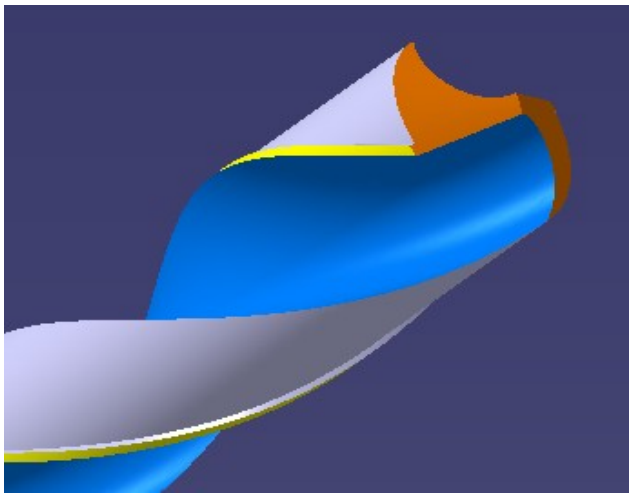

Figure 1-2 Conical point

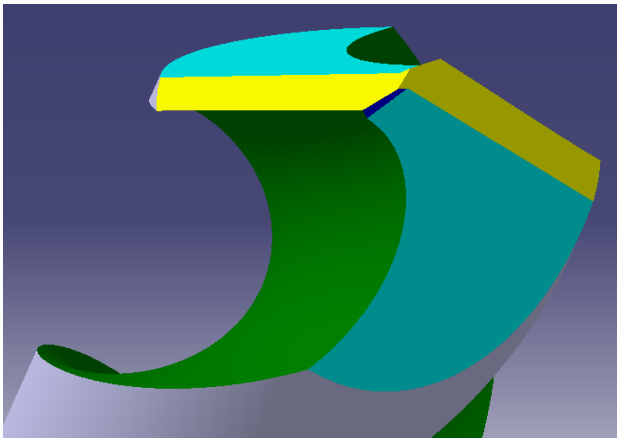

Figure 1-3 Planar point

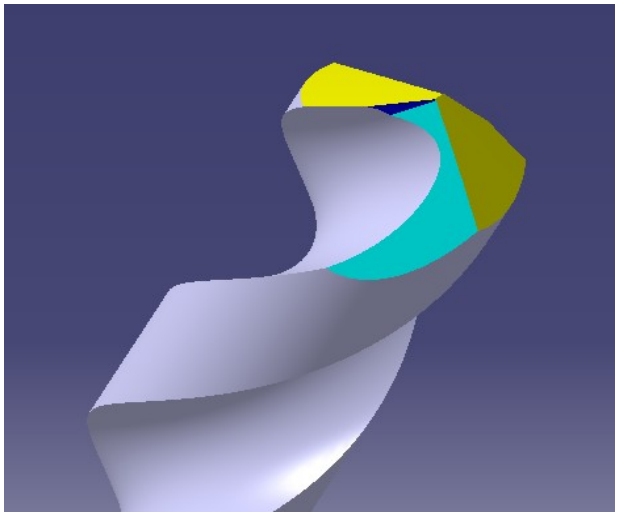

Figure 1-4 Split point

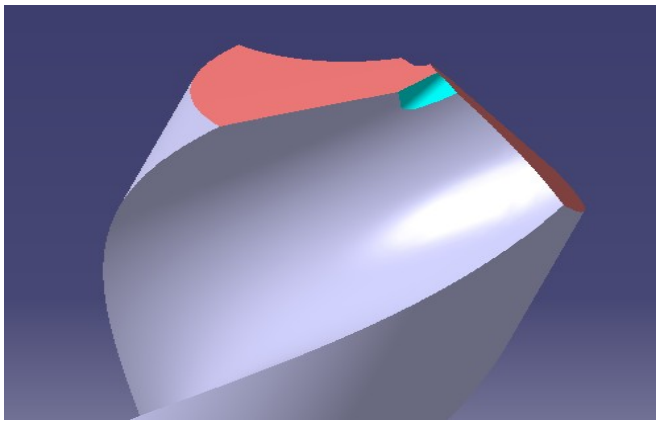

Figure 1-5 Radial (split) point

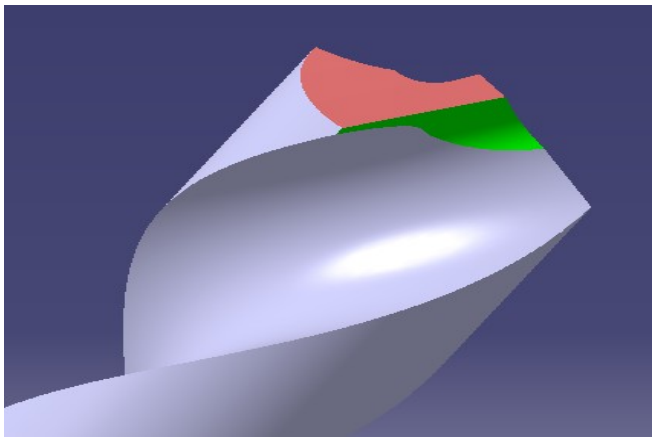

Figure 1-6 Corrected cutting edge point

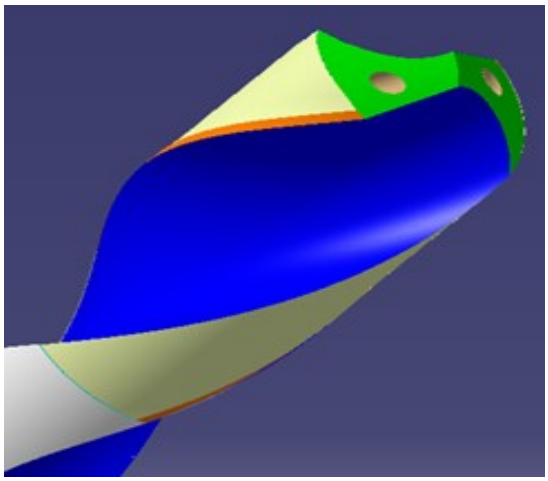

Figure 1-7 Conical point with internal cooling hole

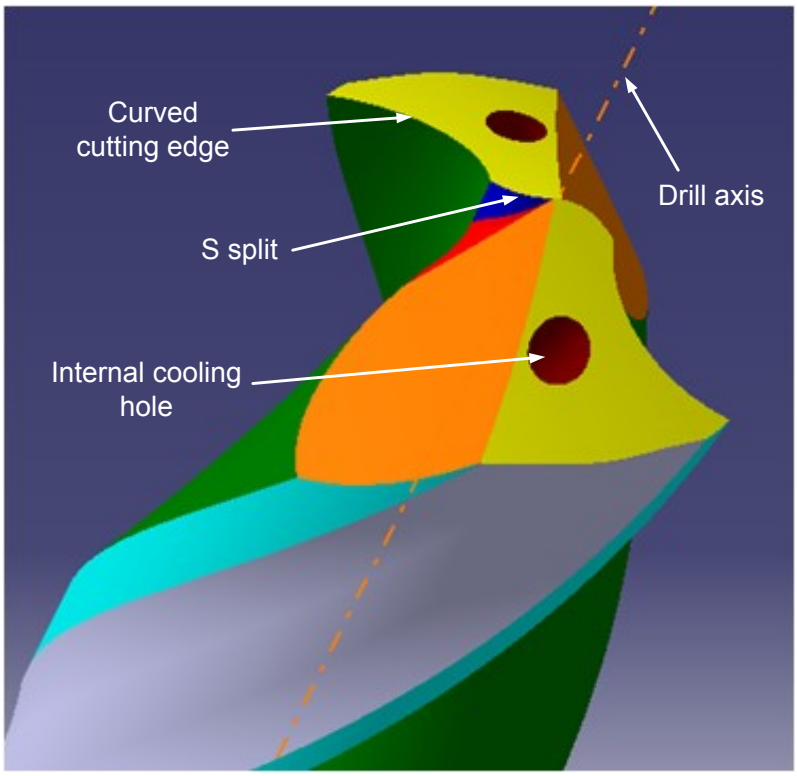

Figure 1-8 Curved cutting edge point with S-split and internal cooling hole

Although drilling seems a relatively simple process, it is really a complex and difficult process. Since drilling occurs inside the workpiece, heat is accumulated, and the cutting temperature could be high, especially, the cutting process contains a large portion of chisel cutting (a cutting process by chisel edge which has more than 45º negative rake angle) or the chips are not small enough. Another problem is lubrication and cooling is difficult to carried out because the chips block the coolant in the flute. To overcome these difficulties, more complex drills have been designed, for example, a Racon point with a round flank, a helical point with a raised tip, a wavy point with a curved cutting lip, and a four-facet split point, etc. It is very important to accurately model drills in 3D for drill analysis. Generally, advanced drill modeling should have two aspects, manufacturing-based design and feature-based modeling.

1.1 Manufacturing-based Design

Manufacturing drill modeling means that the drill modeling should be accurately based on its manufacturing process.

In a new drill design, drill modeling should be always based on what kind of manufacturing process is used to produce a drill. Most drills are machined with grinders. The drill features, for example, the flutes, are part of the envelope surfaces formed by the grinding wheel throughout the grinding route. Thus, drill modeling should always follow the envelope theory, which represents the relationship of the drill shape and its manufacturing process.

In conventional and standard drill analysis, drill modeling should also consider how a grinder machines a drill. Today, the complexity of the drill points and the high labour costs require that the grinding machines must be accurate, versatile, and automated. This requirement leads the appearance of 4-axis, 5-axis and even 6-axis CNC tool-grinding machines. Nowadays most of drills are produced in these multi-axis grinders. The multi-axis grinding machines manufactured by different companies have their own software, which is based on the same or different mathematical models. This means different grinders may use different manufacturing features to machine a drill. So, to accurately built a 3-D solid model, it is very important to know the manufacturing features and the related mathematical models.

1.2 Feature-based Modeling

1.2.1 Definition

A mechanical part consists of several geometric features. Features in geometric feature-based modeling are defined to be parametric shapes associated with geometric parameters (such as length, width, radius etc), positional parameters (such as offset distance, positional angle etc), and orientational parameters (such as orientational angle, right hand of a helix etc). Now, parametric feature-based part design and modeling becomes one of the kernel techniques of the new computer-aided design. It is a dispensable advanced technique since the parametric CAD models of the part features can be easily modified in the part design optimization process. By definition, the parametric feature-based design and modeling is to determine the key feature dimensions as the parameters and to specify the relationships (or constraints) among the parameters and other part dimensions. Fortunately, the functions of defining parameters and constraints are provided in some major CAD/CAM software. Applying these functions, all part dimensions can be calculated by assigning data to the feature parameters and the solid model of the part can be changed accordingly and updated in seconds.

1.2.2 Parametric feature based part design and modeling

Mechanical part design includes a number of decision-making processes and activities. Generally, a mechanical part design has four phases: conceptual solutions, design exploration, design refinement, and final CAD models and engineering drawings. In contrast with the conventional part modeling method which all part dimensions have to be defined independently, parametric feature-based modeling allows the feature parameters and the geometric, positional, and orientational constraints to be specified or related. This can greatly reduce the leading time in part design because the solid 3D CAD model of a part can be easily attained and modified. Generally, four steps are necessary to implement the parametric feature-based part design and modeling, which are

- to define the dimensions of key features as the parameters,
- to define the relationships or constraints between the parameters and the dimensions,
- to establish the 3D solid model with CAD/CAM software, and
- to input the parameters and the constraints in the part model.

Once the parametric feature-based model of a part is built, the part can be changed automatically by assigning different parameter values.

1.3 Literature Review

Many technical articles have discussed about the generalized models of cutting tools, including the mathematical and manufacturing models [2-22]. Engin and Altintas [2] described a mathematical model of general end-mills often used in the industry. For twist drills, the first accurate geometry model was developed by Galloway [3] in 1957. However,

the grinding cone was not unique. In 1973, Armarego et al. [4-5] studied drill point sharpening by the straight lip conical grinding method and developed an analysis of the straight lip conical grinding concept. He discovered the conical grinding processes of flank are determined by four dependent factors, whereas the drill point was specified by three parameters. He gave the relief angle on the flank as the fourth parameter to get the unique solution. A few years later, Tsai and Wu [6] developed a mathematical model that describes drill flank geometry including the conical, hyperbolical, and ellipsoidal drills and the flank of the drill is represented with coincide. This study gives an accurate method to represent the quadratic drill geometry which enables the flank to be analyzed accurately and conveniently by computer. In 1983, Radhakrishnan [7] first derived the mathematical model of the planar split drill point.

Fugelso [8] in 1990 improved the standard straight-cutting-edge model by rotating the drill about its axes by angle ω before sharpening. This improvement solved the problem that the clearance angle is too small near the chisel edge. The new method led to a curved cutting edge, and, from then on, the curve cutting edge was introduced and applied widely in some drilling processes. Lin et al. [9] first developed the helical drill point in 1995 to alleviate the disadvantages of existing planar micro drill point. Ren and Ni [10] developed a new mathematical model for an arbitrary drill flute face by sweeping the polynomial representation of the flute cross-sectional along the helix drill axis with helical movement. The typical mathematical models for multi-facet drills were presented using angle-solid-block method in Ger-Chwang Wang's works [11]. However, the Boolean operation used here can not apply to helical multi-facet point.

In 1988, the direct and the inverse problems related to the flute and grinding wheel were first discussed [12] and then mathematically solved by many researchers. K.F. Ehmann [13] developed a program and presented a well solution for the inverse problem. J.F. Hsieh [14] proposed a general mathematical model of the tool profile and helical drill flank and solved the two problems by using conjugate surface theory.

Along with the development of CAD/CAM technology, CAD approach becomes an attractive way to simulate the geometrical and grinding features of twist drill. Thanks to the objective of the thesis, which is feature-based modeling of the twist drills, eight more related papers are reviewed [15-22]. Based on the Galloway's models, Fujii et al. [15-16] first presented an analysis about the drill point geometry by using computer aided design system. However, the proposed cone parameters were difficult to measure and set. Fuh [17] applied the computer aided design to analyze the quadratic surface model for the twist drill point. Sheth and Malkin [18] reviewed commercial CAD/CAM software for the design and manufacture of components with helical flutes. The CAD system could help engineers design the profile of the tool and the helical flute. Kaldor et al. [19] dealt with geometrical analysis and development for designing the cutter and the grinding wheel profile. The direct and the inverse methods allow prediction of the helical flute profile and the cutter profile, respectively. Kang et al. [20] proposed an analytical solution to helical flute machining through a CAD approach, and a generalized helical flute machining model using the principles of differential geometry and kinematics, was formulated. Vijayaraghavan [21] etc. developed an automated 3D model software based on geometry and manufacturing parameters, and it can be output with solid geometry format which

can be meshed and analyzed in FEA software efficiently. Li e al. [22] presented a method to automatically measure the relief angle and rake angle of the standard twist drill based on 3-D model created by PRO/E. However, the Boolean operation used in [21] and [22] is not feasible in some tangential area.

1.4 Objective of the Thesis

The objectives of the thesis include (a) finding the relationship between the mathematical, manufacturing and geometric models of a twist drill and (b) building a parametric solid model of a twist drill with the CATIA V5 R20 software, based on its machining features. The machining features of the twist drill include the drill body, two flutes, the drill flank, the split (or the gash), and the land. In this work, all the machining features will be parameterized and their solid models will be constructed with the CATIA V5 R20 software.

1.5 Outline of the Thesis

Basically, the document comprises of seven chapters. Chapter one introduces the parametric design and modeling and reviews literature on this topic. Chapter two geometrically models the drill body. Chapter three proposes the parametric modeling for flute grinding with standard wheels in the direct method and renders a new method of determining the grinding wheel profiles of non-standard wheels for machining designed

flutes in the inverse method. Chapter four defines the machining features according their mathematical models and builds the parametric modeling of the flank. Since the main cutting lip is the intersection of the flank face and the flute face, the flank modeling and the flute modeling are very important. Chapter 3 and chapter 4 will describe them in detail. Chapter five constructs the drill split, and in Chapter six, conclusions are drawn for the thesis.

CHAPTER 2 BODY MODELING

2.1Introduction

Body modeling of a twist drill defines the drill's body profile. Only geometrical model is presented for the body modeling.

2.2 Drill Body Parameters

There are five parameters of the drill body, such as the drill diameter, shank diameter, overall length, body length, and backtaper angle.

Table 2-1 Drill body parameters

Parameters	Definition	value
D	Drill diameter	12 mm
D_{shank}	Drill shank diameter	14 mm
L	Drill overall length	120 mm
L_{body}	Drill body length (drill diameter length)	80 mm

DiameterBackTaper	Taper angle of a tapered twist drill body	0.1^{o}

2.3 The procedure of modeling the drill body

All five parameters are used in the twist drill body modeling. These parameters define the correspondingly geometric features. The 3-D model and its key dimensions are shown in Fig 2.1.

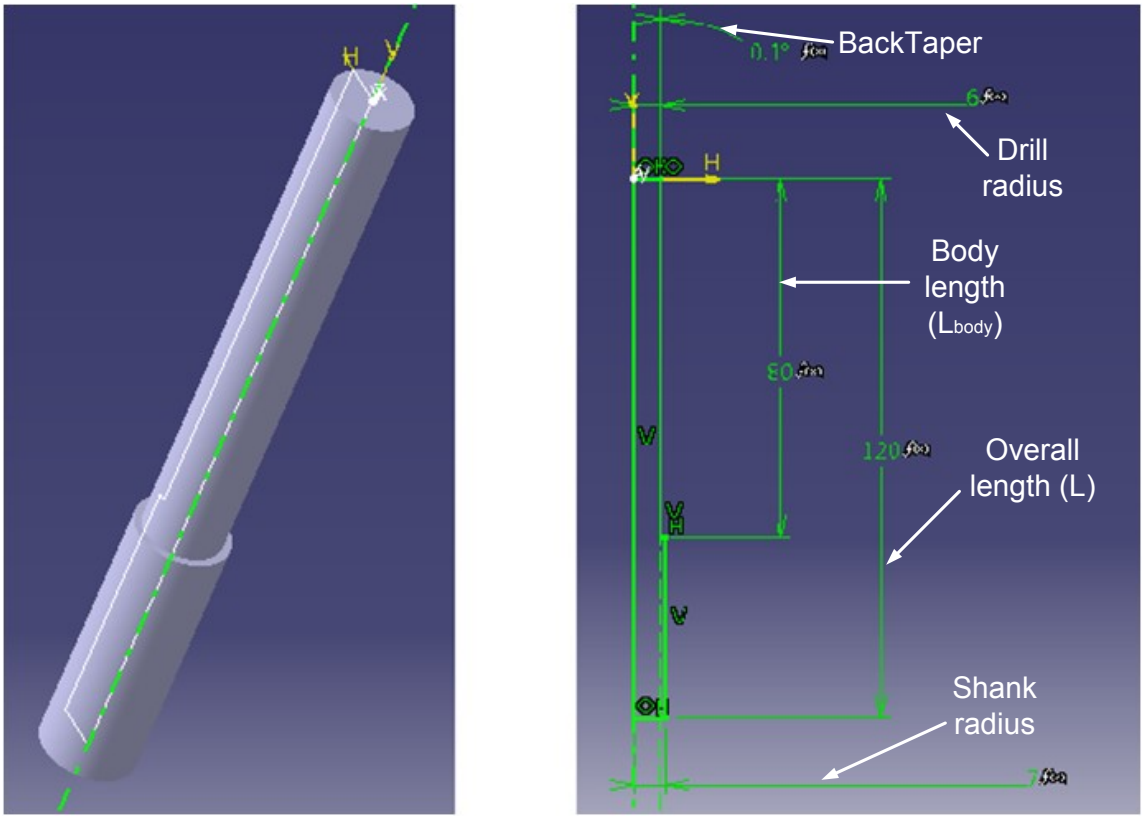

Figure 2-1 Drill body and its key dimensions

Figure 2-2 to 2-7 show the dimensions and corresponding parameters of the twist

drill.

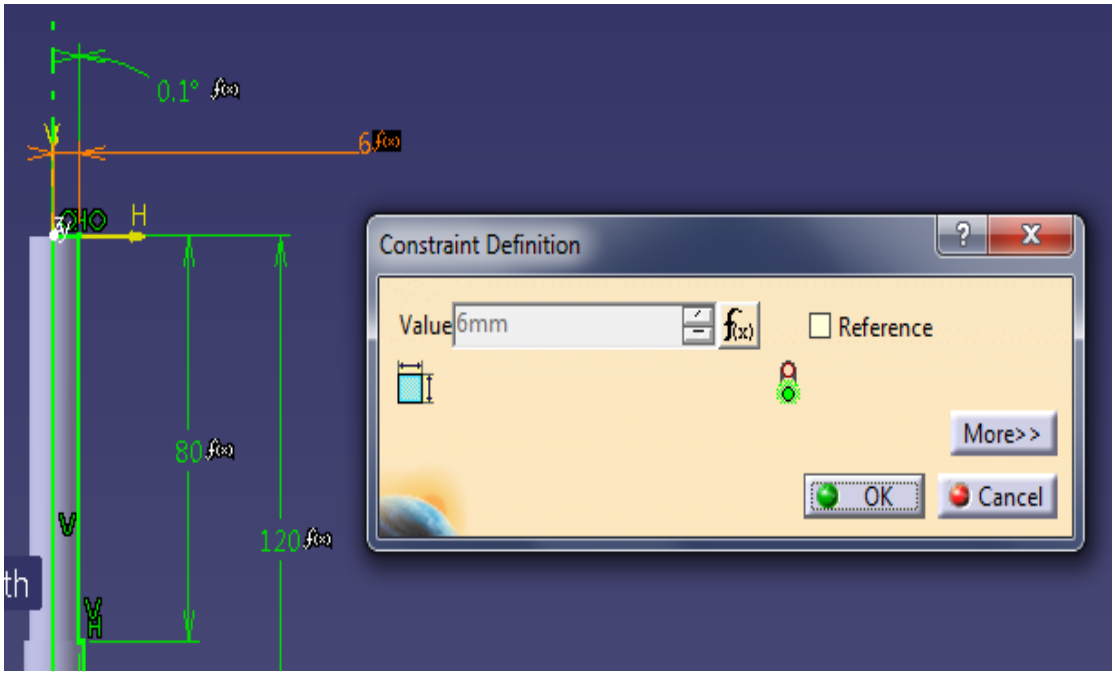

Figure 2-2 Dimension of drill radius

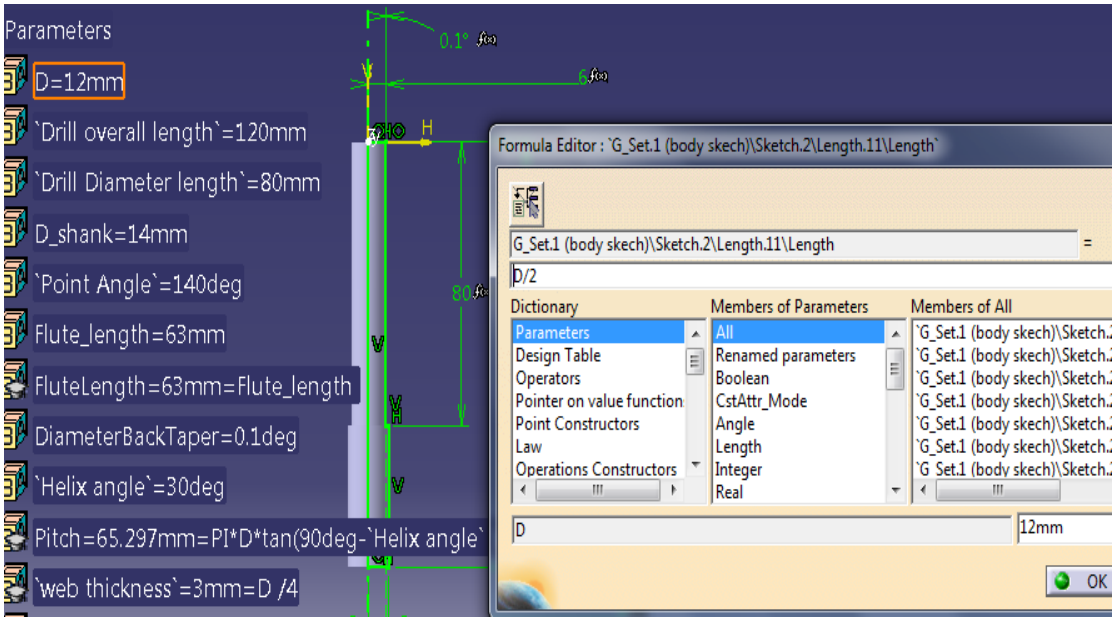

Figure 2-3 Parameter of drill diameter

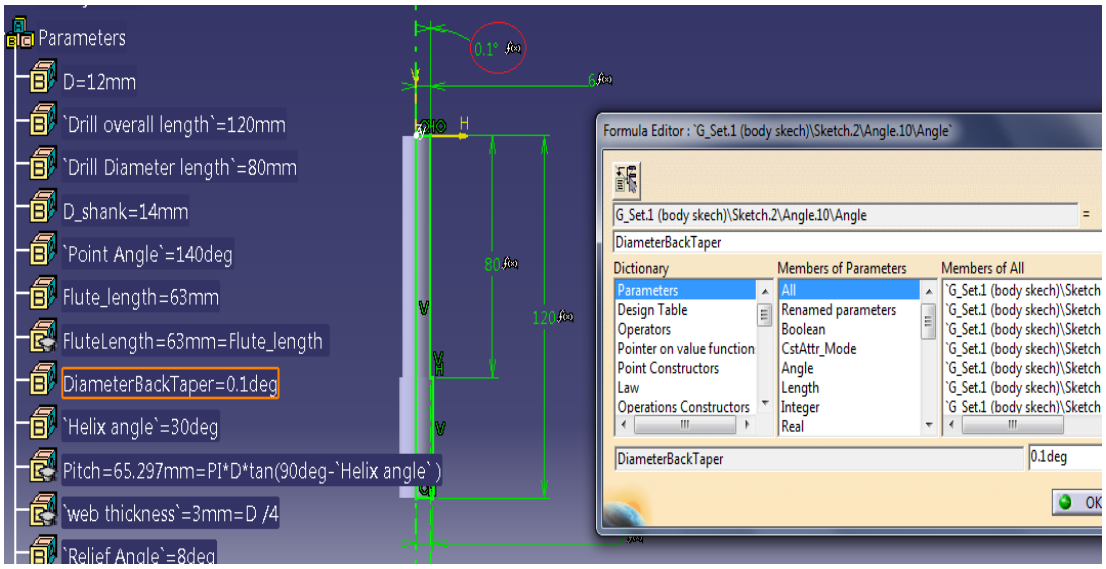

Figure 2-4 Dimension and parameter of drill back taper angle

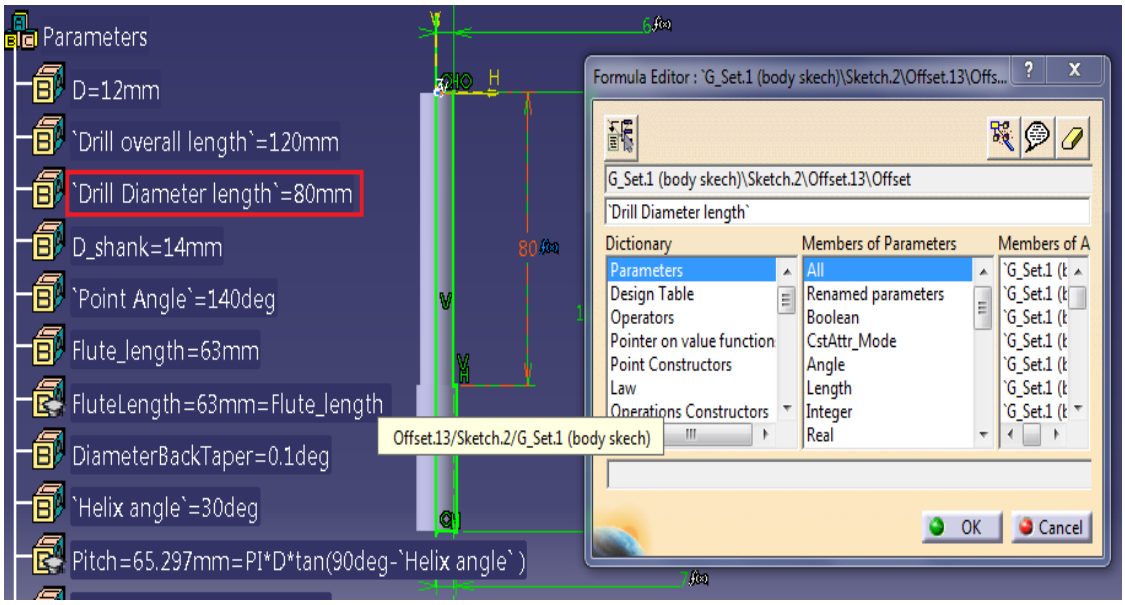

Figure 2-5 Dimension and parameter of drill body length

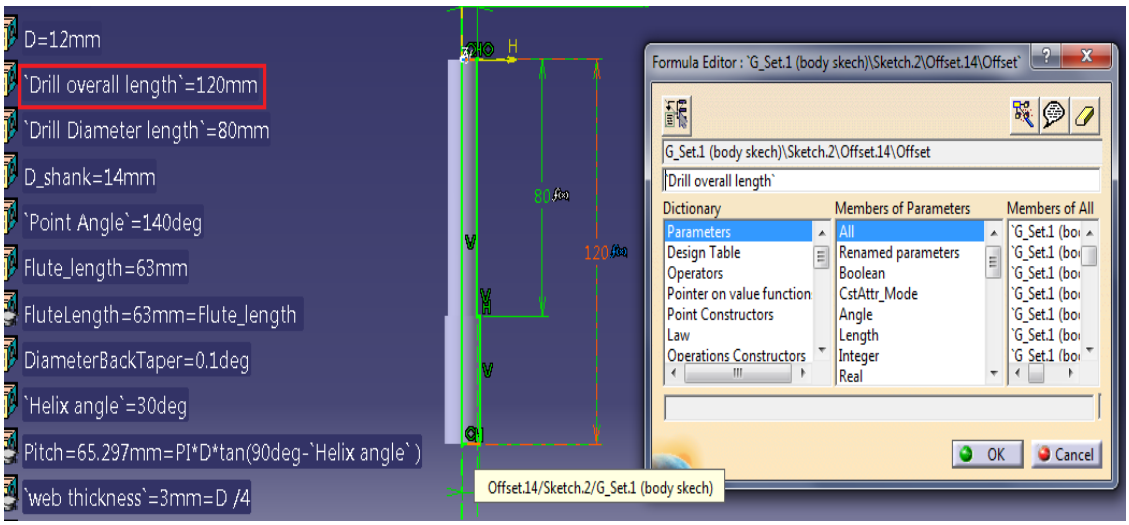

Figure 2-6 Dimension and parameter of drill overall length

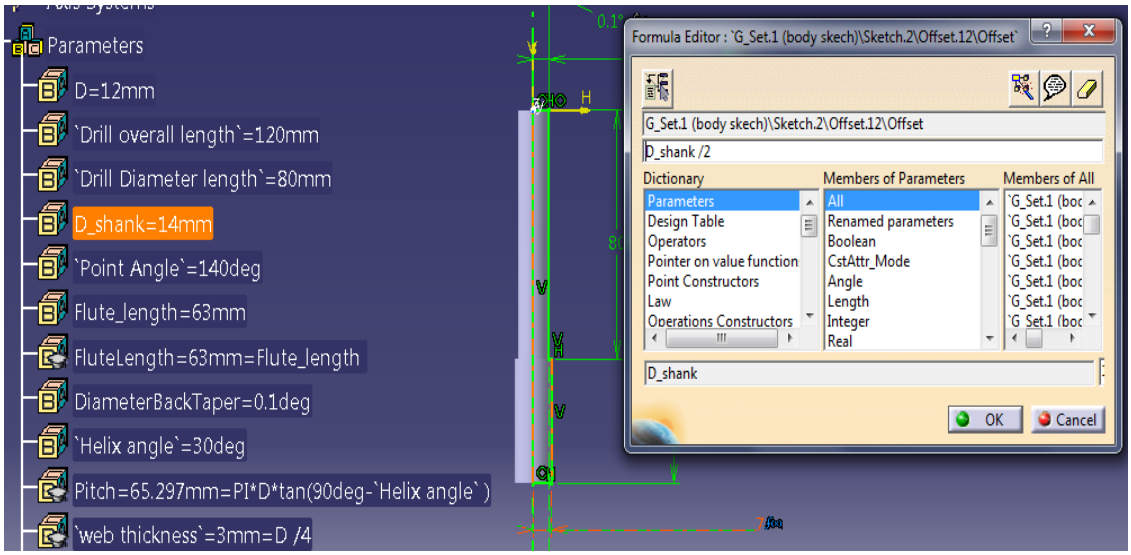

Figure 2-7 Dimension and parameter of drill shank diameter

Chapter 3 Flute Modeling

3.1 Introduction

The flute is one of the most important features of the twist drill. The flute determines the cutting forces and the core size that is very important to the cutter rigidity; and, at the same time, it provides accommodation for chips and evacuates them during machining. For a twist drill, its flutes are vital to the tool rigidity and chip evacuation. However, these two characteristics are contradictory with each other. To attain a tool with high rigidity, the cross section area of the flute and the flute depth should be small so that the core radius is large. On the contrary, to quickly evacuate the chips, the larger the flute space, the quicker the chip flow. It is difficult to optimize the flute shape for highest tool rigidity and fastest chip evacuation. So the flute model that accurately reflects its manufacturing process is very important.

To machine the flutes of the twist drill in practice, there are two different methods, i.e., the direct and the inverse methods. The major difference between these methods is what type of wheel is selected and how the grinding wheel is determined. In the direct method, a standard grinding wheel is first selected; while, in the inverse method, the grinding wheel is nonstandard, and its profile is determined based on a prescribed flute profile. The two methods share the same steps in the flute machining process. In the second step, the cutting edge of the flute is specified as the wheel path. Then, in grinding,

when the wheel moves along the path, it sweeps a volume, in which the stock material is removed, generating the flute. Mathematically, the flute can be represented as part of the outside surface of the wheel swept volume, which is the envelope of the wheel during machining. In this section, a parametric model of the flute is rendered according to the flute manufacturing process.

3.2 The Direct Method of Machining Flutes

The direct method employs standard grinding wheels to grind the flutes. To represent the flutes, the envelope theory should be applied to the standard wheel moving along the pre-determined wheel path, which is the helical cutting edge. As a result, the effective grinding edge can be found, and a mathematical model of the flute can be formulated. In this thesis, two types of standard grinding wheel, which are often used in drill manufacturing, are adopted. A general model of these grinding wheels is built in the following.

3.2.1 Parametric Model of the Standard Grinding Wheels

Two standard grinding wheels used in this work are straight (or parallel) and angled (or bevel) wheels. For the straight wheel, the flanks of both sides of the wheel are straight and normal to the wheel revolving circumference; and, for the angled wheel, one flank of the wheel is straight and the other is inclined with an angle to the wheel circumference.

Usually, these types of grinding wheels are popular and economic, and they are easy to dress after the wheel worn out. Figure 3.1 illustrates the two grinding wheels with the parameters. Of the two wheels, the angled wheel is more generic in shape, and the parametric equation of the angled wheel can represent the straight wheel by setting the angle to 90^{o}.

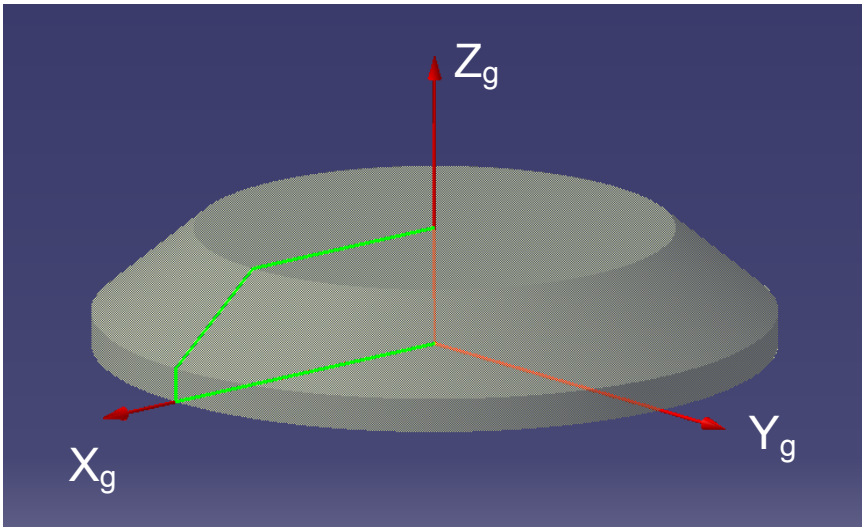

Figure 3-1 The profile of a standard angled grinding wheel

To derive the parametric equation of the angled wheel, a grinding wheel coordinate system $\left(x_g y_g z_g\right)$ is established in such a way that the origin is at the center of the straight flank face, the z_g axis is aligned with the wheel axis and points inside the wheel, and the x_g and y_g are perpendicular to each other ad on the straight flank face (see Figure 3.1). The profile of the grinding wheel is a polygon $\mathbf{H_0H_1H_2H_3H_4}$ and is shown on plane $x_g z_g$ in Figure 3.2.

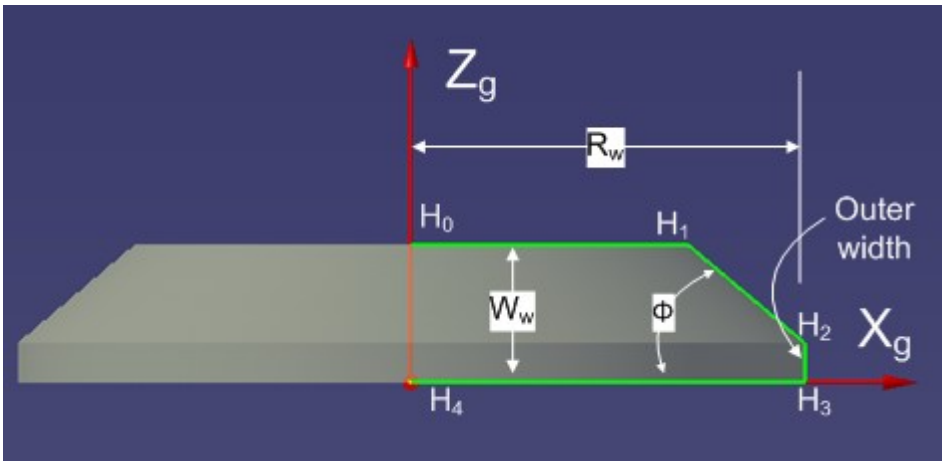

Figure 3-2 The parameters of the grinding wheel profile.

The radius of the wheel circumference is R_w, the thickness of the wheel is W_w, and the inclined angle of the edge is ϕ. The lengths starting from **H_0** to the five vertexes in the polygon are denoted as L_0, L_1, L_2, L_3, and L_4, where L_0 is zero. The coordinates of **H_0**, **H_1**, **H_2**, **H_3**, and **H_4** are $[0,\ 0,\ W_w]^T$, $[L_1,\ 0,\ W_w]^T$, $\left[L_1+(L_2-L_1)\cos\phi,\ 0,\ W_w-(L_2-L_1)\sin\phi\right]^T$, $[L_3,\ 0,\ 0]^T$, and $[0,\ 0,\ 0]^T$, respectively. To find the parametric equation of the polygon edges, a parameter, *h*, the length on the polygon starting from **H_0** is used. Then the equations of the polygon edges with parameter, *h*, are derived as

For edge H_0H_1, $\quad 0 < h \le L_1 \qquad {}^g\mathbf{q}_1 = \begin{bmatrix} h \\ 0 \\ W_w \\ 1 \end{bmatrix}$;

For edge H_1H_2, $\quad L_1 < h \le L_2 \qquad {}^g\mathbf{q}_2 = \begin{bmatrix} L_1+(h-L_1)\cos\phi \\ 0 \\ W_w-(h-L_1)\sin\phi \\ 1 \end{bmatrix}$;

For edge H_2H_3, $L_2 < h \le L_3$ $\quad {}^g\mathbf{q}_3 = \begin{bmatrix} R_w \\ 0 \\ L_3 - h \\ 1 \end{bmatrix}$;

For edge H_3H_4, $L_3 < h \le L_4$ $\quad {}^g\mathbf{q}_4 = \begin{bmatrix} L_4 - h \\ 0 \\ 0 \\ 1 \end{bmatrix}$;

The wheel is constructed by rotating the profile polygon about z_g by 360 degrees. Suppose the rotation angle *v* starts from axis x_g and is a parameter of the wheel surface, the rotation matrix and the parametric equations of the wheel surface are formulated as

The general surface equation is

$$
\begin{aligned}
{}^g\mathbf{r} = \begin{bmatrix} {}^gr_x \\ {}^gr_y \\ {}^gr_z \\ 1 \end{bmatrix} &= \begin{bmatrix} \cos v & -\sin v & 0 & 0 \\ \sin v & \cos v & 0 & 0 \\ 0 & 0 & 1 & 0 \\ 0 & 0 & 0 & 1 \end{bmatrix} {}^gq \\
&= \begin{bmatrix} x\,{}^g(h)\cdot\cos v & {}^gx(h)\cdot\sin v & {}^gz(h) & 1 \end{bmatrix}^T
\end{aligned}
\tag{3.1}
$$

Thus,

- For surface ${}^gS_1(h,v)$ generated with H_0H_1 ,

$$
{}^g\mathbf{S}_1(h,v) = \begin{bmatrix} h\cdot\cos v \\ h\cdot\sin v \\ W_w \\ 1 \end{bmatrix} \tag{3.2}
$$

where $0 < h \le \mathrm{L}_1$ and $0 \le v \le 360^\circ$;

- For surface ${}^gS_2(h,v)$ generated with H_1H_2,

$$ {}^{g}\mathbf{S}_2(h,v) = \begin{bmatrix} \left(L_1 + (h - L_1)\cdot\cos\phi\right)\cdot\cos v \\ \left(L_1 + (h - L_1)\cdot\cos\phi\right)\cdot\sin v \\ W_w - (h - L_1)\cdot\sin\phi \\ 1 \end{bmatrix} \tag{3.3} $$

where $L_1 < h \le L_2$ and $0 \le v \le 360^\circ$;

- For surface ${}^{g}S_3(h,v)$ generated with H_2H_3,

$$ {}^{g}\mathbf{S}_3(h,v) = \begin{bmatrix} R_w\cos v \\ R_w\sin v \\ H_3 - h \\ 1 \end{bmatrix} \tag{3.4} $$

where $L_2 < h \le L_3$ and $0 \le v \le 360^\circ$;

- For surface ${}^{g}S_4(h,v)$ generated with H_3H_4,

$$ {}^{g}\mathbf{S}_4(h,v) = \begin{bmatrix} (L_4 - h)\cos v \\ (L_4 - h)\sin v \\ 0 \\ 1 \end{bmatrix} \tag{3.5} $$

where $L_3 < h \le L_4$ and $0 \le v \le 360^\circ$.

3.2.2 Mathematical Model of the Multi-axis CNC Grinding Process

To truly represent the geometry of a machined flute, a mathematical model of the multi-axis CNC grinding process for the flute is necessary, which is established here according to the kinematics of the ANCA CNC tool grinding machine used to cut the flute.

In the actual flute grinding process, the wheel axis could be in a skew orientation in terms of the cutter axis, which is usually in horizontal, and the cutter is simultaneously rotated and fed along its axis. Although the grinding kinematics is that both the wheel and the cutter move at the same time, it can be converted to an equivalent kinematics that the cutter is stationary and the wheel moves and rotates for the same flute geometry. Thus, the cutter flute can be modeled by representing the wheel in the flute machining process in the cutter coordinate system.

In the equivalent grinding kinematics, first, the cutter coordinate system $(x_d y_d z_d)$ is fixed, and the grinding wheel coordinate system $(x_g y_g z_g)$ is coincided with it before grinding. During machining, the rotation angle θ of the cutter changes, and the wheel location and orientation change accordingly, which can be decomposed in the following steps.

The wheel coordinate system is translated along its axis z_g by Δz_g, which is equal to $k_z\theta$. k_z is the coefficient related with the helix angle of the cutting edge. The translation matrix is $\mathbf{M}^{\mathrm{T}}(0,0,\Delta z_g)=\begin{bmatrix}1&0&0&0\\0&1&0&0\\0&0&1&\Delta z_g\\0&0&0&1\end{bmatrix}$.

The wheel coordinate system is rotated about its z_g axis by θ. The rotation matrix is $\mathbf{M}^{\mathrm{R}}(z_g,\theta)=\begin{bmatrix}\cos\theta&-\sin\theta&0&0\\\sin\theta&\cos\theta&0&0\\0&0&1&0\\0&0&0&1\end{bmatrix}$.

The wheel coordinate system is translated along its x_g axis by Δx_g, which is equal to $(\mathrm{R_w}+r_c)+k_x\cdot\theta$. k_x is related with the taper angle of the cutter, if it is a tapered twist

drill. The translation matrix is $\mathbf{M}^{T}\left(\Delta x_g, 0, 0\right) = \begin{bmatrix} 1 & 0 & 0 & \Delta x_g \\ 0 & 1 & 0 & 0 \\ 0 & 0 & 1 & 0 \\ 0 & 0 & 0 & 1 \end{bmatrix}$.

The wheel coordinate system is rotated about its axis x_g by angle β. The rotation matrix is $M^{R}\left(x_g, \beta\right) = \begin{bmatrix} 1 & 0 & 0 & 0 \\ 0 & \cos\beta & -\sin\beta & 0 \\ 0 & \sin\beta & \cos\beta & 0 \\ 0 & 0 & 0 & 1 \end{bmatrix}$.

The wheel coordinate system is rotated about its y_g axis by angle α. The rotation matrix is $M^{R}\left(y_g, \alpha\right) = \begin{bmatrix} \cos\alpha & 0 & \sin\alpha & 0 \\ 0 & 1 & 0 & 0 \\ -\sin\alpha & 0 & \cos\alpha & 0 \\ 0 & 0 & 0 & 1 \end{bmatrix}$

Figure 3-3 illustrates the first three steps of the kinematics when θ is equal to 360 degrees. Using Euler rule, the equivalent matrix of the five transformation matrices can be derived as

$$ {}^{d}_{g}M = M^{T}(0,0,\Delta z_g)M^{R}(z_g,\theta)M^{T}(\Delta x_g,0,0)M^{R}(x_g,\beta)M^{R}(y_g,\alpha) $$

$$ = \begin{bmatrix} \cos\theta\cos\alpha - \sin\theta\sin\beta\sin\alpha & -\sin\theta\cos\beta & \cos\theta\sin\alpha + \sin\theta\sin\beta\cos\alpha & \Delta x_g\cos\theta \\ \sin\theta\cos\alpha + \cos\theta\sin\beta\sin\alpha & \cos\theta\cos\beta & \sin\theta\sin\alpha - \cos\theta\sin\beta\cos\alpha & \Delta x_g\sin\theta \\ -\cos\beta\sin\alpha & \sin\beta & \cos\beta\cos\alpha & \Delta z_g \\ 0 & 0 & 0 & 1 \end{bmatrix} \quad (3.6) $$

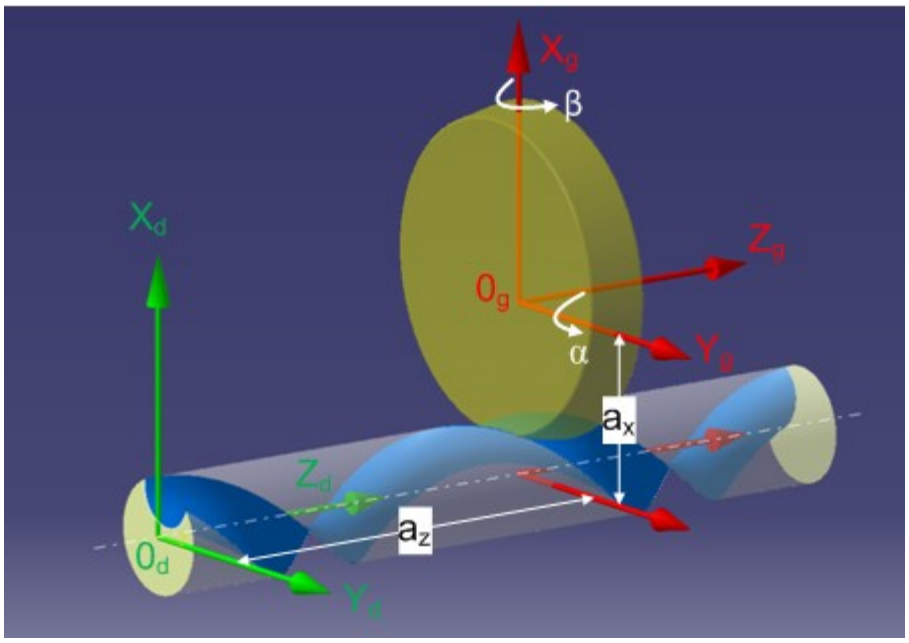

Figure 3-3 Illustration of the kinematics of multi-axis grinding of flutes

Applying this equivalent matrix of the machining kinematics, the wheel surfaces can be represented in the cutter coordinate system while the wheel cuts the flute. The general equation is

$$ {}^{d}\mathbf{S}(h,v) = {}^{d}_{g}\mathbf{M}(\theta,\alpha,\beta,k_x,k_z)\cdot {}^{g}\mathbf{S}(h,v) \tag{3.7} $$

In detail, the wheel surfaces can be found in the cutter coordinate system as

The equation of surface ${}^{g}\mathbf{S}_1(h,v)$ in the cutter coordinate system is

$$ {}^{d}\mathbf{S}_1(h,v) = \begin{bmatrix} x_1(h,v) \\ y_1(h,v) \\ z_1(h,v) \end{bmatrix} = \begin{bmatrix} h\cdot\cos\theta\cdot\cos v - h\cdot\sin\theta\cdot\cos\beta\cdot\sin v + W_w\cdot\sin\theta\cdot\sin\beta + \Delta x_g\cdot\cos\theta \\ h\cdot\sin\theta\cdot\cos v + h\cdot\cos\theta\cdot\cos\beta\cdot\sin v - W_w\cdot\cos\theta\cdot\sin\beta + \Delta x_g\cdot\sin\theta \\ h\cdot\sin\beta\cdot\sin v + W_w\cdot\cos\beta + k_z\cdot\theta \end{bmatrix} \tag{3.8} $$

where $0 < h \le \mathrm{L}_1$ and $0 \le v \le 360^\circ$;

The equation of surface ${}^{g}\mathbf{S}_2(h,v)$ in the cutter coordinate system is

$$
\begin{aligned}
{}^{d}\mathbf{S}_2(h,v) &= \begin{bmatrix} x_2(h,v) \\ y_2(h,v) \\ z_2(h,v) \end{bmatrix} \\
&= \begin{bmatrix} \left(\mathrm{L}_1 + (h-\mathrm{L}_1)\cdot\cos\phi\right)\cdot\left(\cos\theta\cdot\cos v - \sin\theta\cdot\cos\beta\cdot\sin v\right) + \left(W_w - (h-\mathrm{L}_1)\cdot\sin\phi\right)\cdot\sin\theta\cdot\sin\beta + \Delta x_g\cdot\cos\theta \\ \left(\mathrm{L}_1 + (h-\mathrm{L}_1)\cdot\cos\phi\right)\cdot\left(\sin\theta\cdot\cos v + \cos\theta\cdot\cos\beta\cdot\sin v\right) - \left(W_w - (h-\mathrm{L}_1)\cdot\sin\phi\right)\cdot\cos\theta\cdot\sin\beta + \Delta x_g\cdot\sin\theta \\ \left(\mathrm{L}_1 + (h-\mathrm{L}_1)\cdot\cos\phi\right)\cdot\sin\beta\cdot\sin v + \left(W_w - (h-\mathrm{L}_1)\cdot\sin\phi\right)\cdot\cos\beta + k_z\cdot\theta \end{bmatrix}
\end{aligned}
\tag{3.9}
$$

where $\mathrm{L}_1 < h \le \mathrm{L}_2$ and $0 \le v \le 360^\circ$;

The equation of surface ${}^{g}\mathbf{S}_3(h,v)$ in the cutter coordinate system is

$$
\begin{aligned}
{}^{d}\mathbf{S}_3(h,v) &= \begin{bmatrix} x_3(h,v) \\ y_3(h,v) \\ z_3(h,v) \end{bmatrix} \\
&= \begin{bmatrix} R_w\cdot\left(\cos\theta\cdot\cos v - \sin\theta\cdot\cos\beta\cdot\sin v\right) + \left(\mathrm{L}_3 - h\right)\cdot\sin\theta\cdot\sin\beta + \Delta x_g\cdot\cos\theta \\ R_w\cdot\left(\sin\theta\cdot\cos v + \cos\theta\cdot\cos\beta\cdot\sin v\right) - \left(\mathrm{L}_3 - h\right)\cdot\cos\theta\cdot\sin\beta + \Delta x_g\cdot\sin\theta \\ R_w\cdot\sin\beta\cdot\sin v + \left(\mathrm{L}_3 - h\right)\cdot\cos\beta + k_z\cdot\theta \end{bmatrix}
\end{aligned}
\tag{3.10}
$$

where $\mathrm{L}_2 < h \le \mathrm{L}_3$ and $0 \le v \le 360^\circ$;

The equation of surface ${}^{g}\mathbf{S}_4(h,v)$ in the cutter coordinate system is

$$
{}^{d}\mathbf{S}_4(h,v) = \begin{bmatrix} x_4(h,v) \\ y_4(h,v) \\ z_4(h,v) \end{bmatrix} = \begin{bmatrix} \left(\mathrm{L}_4 - h\right)\cdot\left(\cos\theta\cdot\cos v - \sin\theta\cdot\cos\beta\cdot\sin v\right) + \Delta x_g\cdot\cos\theta \\ \left(\mathrm{L}_4 - h\right)\cdot\left(\sin\theta\cdot\cos v + \cos\theta\cdot\cos\beta\cdot\sin v\right) + \Delta x_g\cdot\sin\theta \\ \left(\mathrm{L}_4 - h\right)\cdot\sin\beta\cdot\sin v + k_z\cdot\theta \end{bmatrix} \tag{3.11}
$$

where $\mathrm{L}_3 < h \le \mathrm{L}_4$ and $0 \le v \le 360^\circ$.

3.2.3 Parametric equation of effective grinding edge

In the multi-axis CNC grinding of a flute, a complex volume swept by the wheel while

moving and rotating alone the cutter, and the stock material within the volume is removed. Eventually, a flute is formed. Geometrically, the volume outside surface is the envelope of all the geometries of the wheel at different locations and in different orientations. In this work, the volume is called wheel swept volume, and its surface is called wheel swept surface. Using the well established envelope theory, the wheel swept surface can be formulated. Specifically, at a moment of the machining, there are a group of wheel points, at each of which the wheel surface normal is perpendicular to the instantaneous wheel feeding direction. These wheel points define a curve on the wheel that is called effective grinding edge in this work. The effective grinding edge is the curve of the wheel swept surface at that moment. Thus, in the cutter coordinate system, the general equation of effective grinding edge is

$$\left[\frac{\partial^d \mathbf{S}(h,v)}{\partial h}\times\frac{\partial^d \mathbf{S}(h,v)}{\partial v}\right]\cdot\frac{\partial^d \mathbf{S}(h,v)}{\partial \theta}=0 \qquad (3.12)$$

Since the wheel includes four surfaces, the effective grinding edge consists of four pieces, and their equations are

For $0<h\le \mathrm{L}_1$, the effective grind edge equation is

$$f_1(h,v)=h\cdot\sin\beta\cdot\cos v+\Delta x_g\cdot\sin\beta-k_z\cdot\cos\beta=0\ . \qquad (3.13)$$

For $\mathrm{L}_1<h\le \mathrm{L}_2$, the effective grinding edge is

$$f_2(h,v)=k_z\cdot\cos\phi\cdot\cos\beta+k_z\cdot\sin\beta\cdot\sin\phi\cdot\sin v+\mathrm{L}_1\cdot\cos v\cdot\sin\beta-\mathrm{L}_1\cdot\cos\phi\cdot\cos v\cdot\sin\beta$$
$$+W_w\cdot\sin\beta\cdot\cos v\cdot\sin\phi-h\cdot\sin\beta\cdot\cos v+\Delta x_g\cdot\cos\beta\cdot\sin\phi\cdot\sin v-\Delta x_g\cdot\cos\phi\cdot\sin\beta=0 \qquad (3.14)$$

For $\mathrm{L}_2<h\le \mathrm{L}_3$, the effective grinding edge is

$$f_3(h,v)=\mathrm{L}_3\cdot\sin\beta\cdot\cos v+k_z\cdot\sin\beta\cdot\sin v-h\cdot\sin\beta\cdot\cos v+\Delta x_g\cdot\cos\beta\cdot\sin v=0\ .(3.15)$$

For $\mathrm{L}_3<h\le\mathrm{L}_4$, the effective grinding edge is

$$\begin{aligned}f_4(h,v)=&\Delta x_g\cdot\mathrm{L}_4\cdot sin\beta-k_z\cdot\mathrm{L}_4\cdot cos\beta+\mathrm{L}_4^2\cdot\cos v\cdot sin\beta+h^2\cdot\cos v\cdot sin\beta\\&+k_z\cdot h\cdot cos\beta-\Delta x_g\cdot h\cdot sin\beta-2\cdot\mathrm{L}_4\cdot h\cdot\cos v\cdot sin\beta=0\end{aligned}\quad .\quad (3.16)$$

With the four equations, the four pieces of an effective grinding edge at a machining time can be found. By repeating this step at all the machine times, the wheel swept surface can be found, thus, the flute is represented. In general, in the multi-axis CNC grinding of flutes, the wheel orientation remains the same in the process, so the effective grinding edge keeps the same shape along the flute. The effective grinding edge has to be found once, instead of at every machining time. Therefore, the machined flute can be generated by sweeping the effective grinding edge along the cutting edge.

3.2.4 Flute Cross-Sectional Profile

In this work, an actual flute cross-sectional profile refers to the intersection between the machined flute model and a plane perpendicular to the cutter axis. An effective grinding edge is a 3-dimensional curve, and the actual flute cross-sectional profile is a 2-dimensional curve. In practice, the cutter sometimes is designed, in which the flute cross-sectional profile is given. To check the machining accuracy, the design and the actual flute cross-sectional profiles are compared to find their maximum deviation. With the equation of the effective grinding edge of the wheel at a machining time, the mathematical model the flute profile at the ^{d}z equal to zero can be derived. Similarly, the profile consists of four segments due to the four wheel surfaces.

For $0 < h \le L_1$, and $-\Delta\theta \le \theta \le \Delta\theta$, the parameters of the points of the flute profile can found by solving the system of equations, Eq. 3.16,

$$\begin{cases} f_1(h,v) = 0 \\ h \cdot \sin\beta \cdot \sin v + W_w \cdot \cos\beta + k_z \cdot \theta = 0 \end{cases}. \tag{3.17}$$

For $L_1 < h \le L_2$, and $-\Delta\theta \le \theta \le \Delta\theta$, the parameters of the points of the flute profile can be found by solving the system of equations, Eq. 3.17,

$$\begin{cases} f_2(h,v) = 0 \\ \left(L_1 + (h - L_1) \cdot \cos\phi\right) \cdot \sin\beta \cdot \sin v + \left(W_w - (h - L_1) \cdot \sin\phi\right) \cdot \cos\beta + k_z \cdot \theta = 0 \end{cases}. \tag{3.18}$$

For $L_2 < h \le L_3$, and $-\Delta\theta \le \theta \le \Delta\theta$, the parameters of the points of the flute profile can be found by solving the system of equations, Eq. 3.18,

$$\begin{cases} f_3(h,v) = 0 \\ R_w \cdot \sin\beta \cdot \sin v + (L_3 - h) \cdot \cos\beta + k_z \cdot \theta = 0 \end{cases}. \tag{3.19}$$

For $L_3 < h \le L_4$, and $-\Delta\theta \le \theta \le \Delta\theta$, the parameters of the points of the flute profile can be found by solving the system of equations, Eq. 3.19,

$$\begin{cases} f_4(h,v) = 0 \\ (L_4 - h) \cdot \sin\beta \cdot \sin v + k_z \cdot \theta = 0 \end{cases}. \tag{3.20}$$

After solving the systems of equations, the parameters of the profile points can be attained, and the coordinates of the profile points in the cutter coordinate system can be calculated by substituting the parameter values to Eqs. 3.13-3.16.

3.2.5 Application of the Direct Method

The direct method of grinding flutes is rendered with all theoretical formula in the

above sections. To demonstrate its validity, the direct method is applied to several practical examples. In these examples, a solid carbide twist drill with the diameter of 20 mm and the cutting edge helix angle of 30 degrees is adopted. Three grinding wheels with different parameter values are used to machine the flutes of the twist drill. The parameter values of these wheels are listed in Table 3.1, and the illustrative diagram of the wheel is plotted in Fig. 3-4.

Table 3-1 The parameter values of the grinding wheels used to cut the drill flutes

Grinding wheel No.	Wheel radius R_w (mm)	Wheel width W_w (mm)	Wheel outer width W_o (mm)	Wheel angle ϕ (deg.)
1	75	18	1	45
2	75	18	1	55
3	75	18	1	65

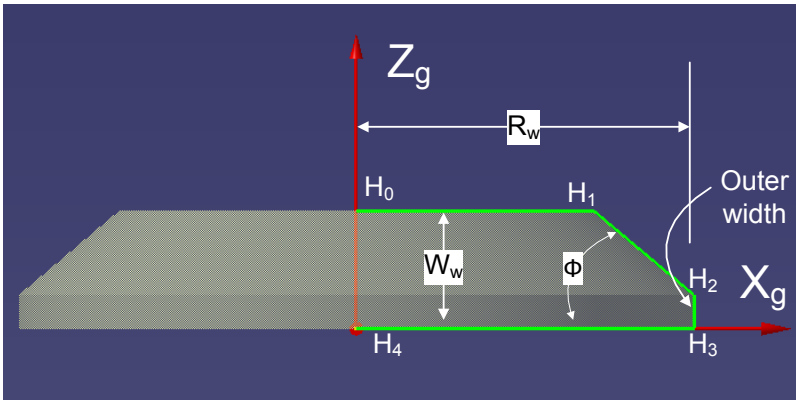

Figure 3-4 The parameters of the grinding wheel profile.

In the first example, the No. 1 grinding wheel is used to machine the drill flute. The generated flute and the cross section of the flute are shown in Fig. 3-5.

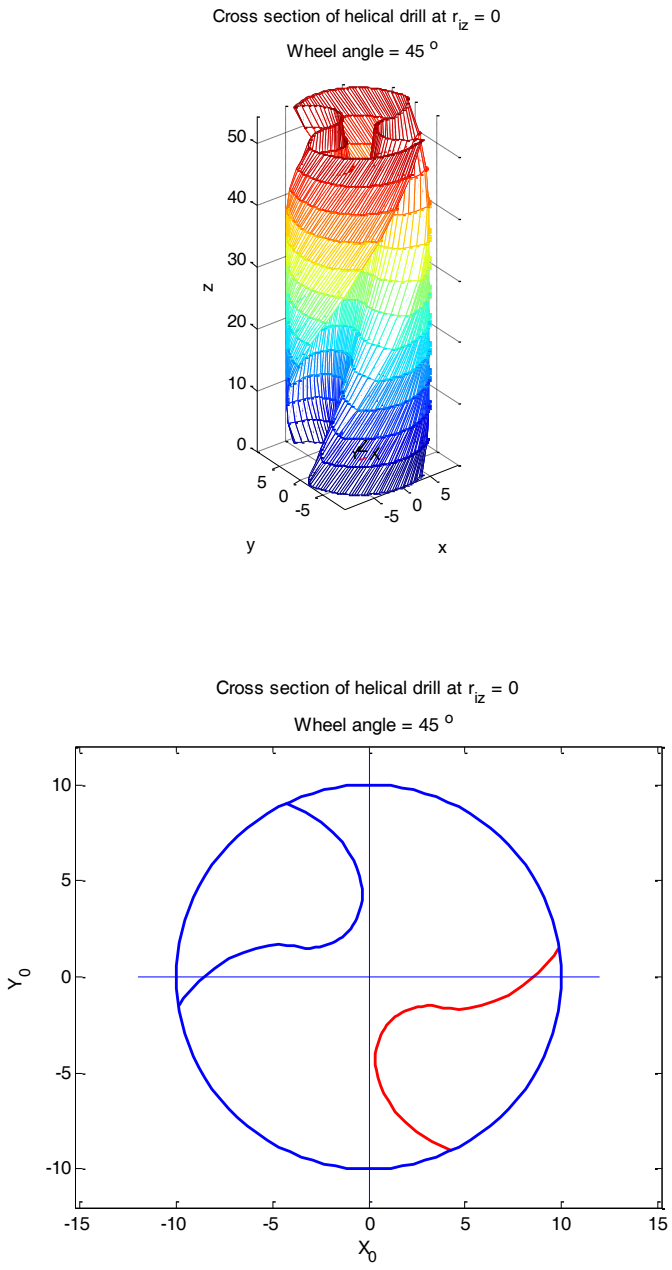

Figure 3-5 The three-dimensional flute and its cross section of the drill machined using the No. 1 grinding wheel.

In the second example, the No. 2 grinding wheel is used to machine the drill flute. The generated flute and the cross section of the flute are shown in Fig. 3-6.

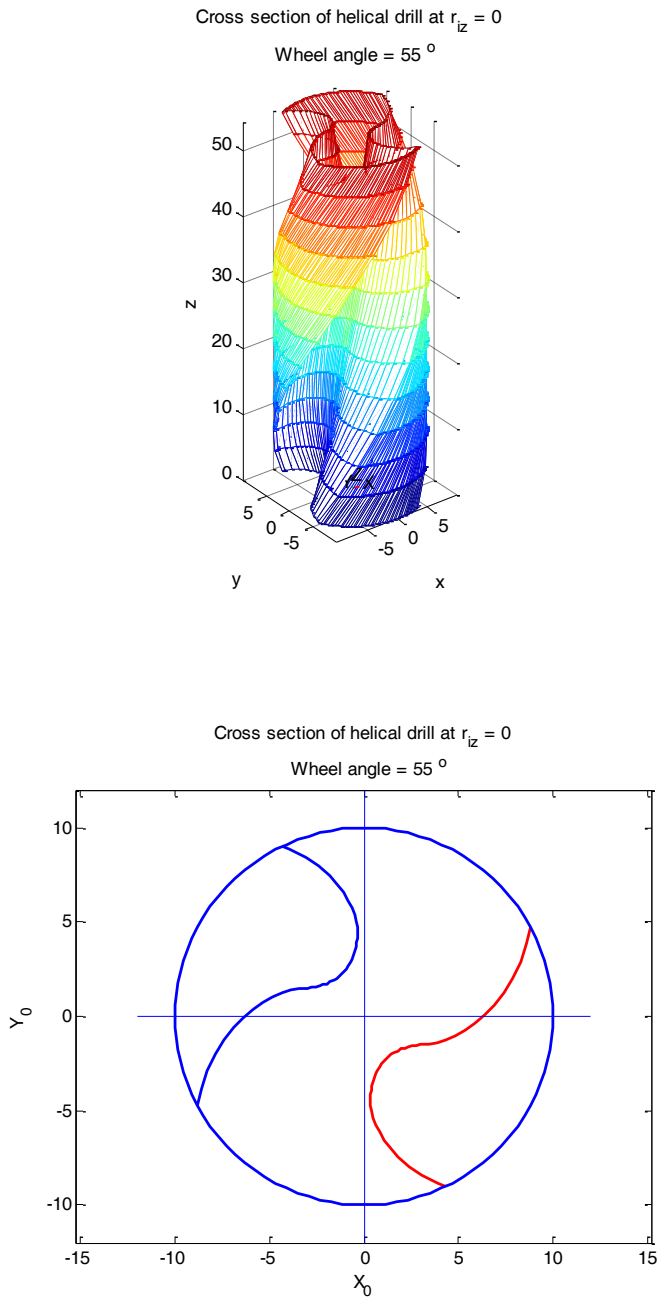

Figure 3-6 The three-dimensional flute and its cross section of the drill machined using the No. 2 grinding wheel.

In the second example, the No. 3 grinding wheel is used to machine the drill flute. The generated flute and the cross section of the flute are shown in Fig. 3-7.

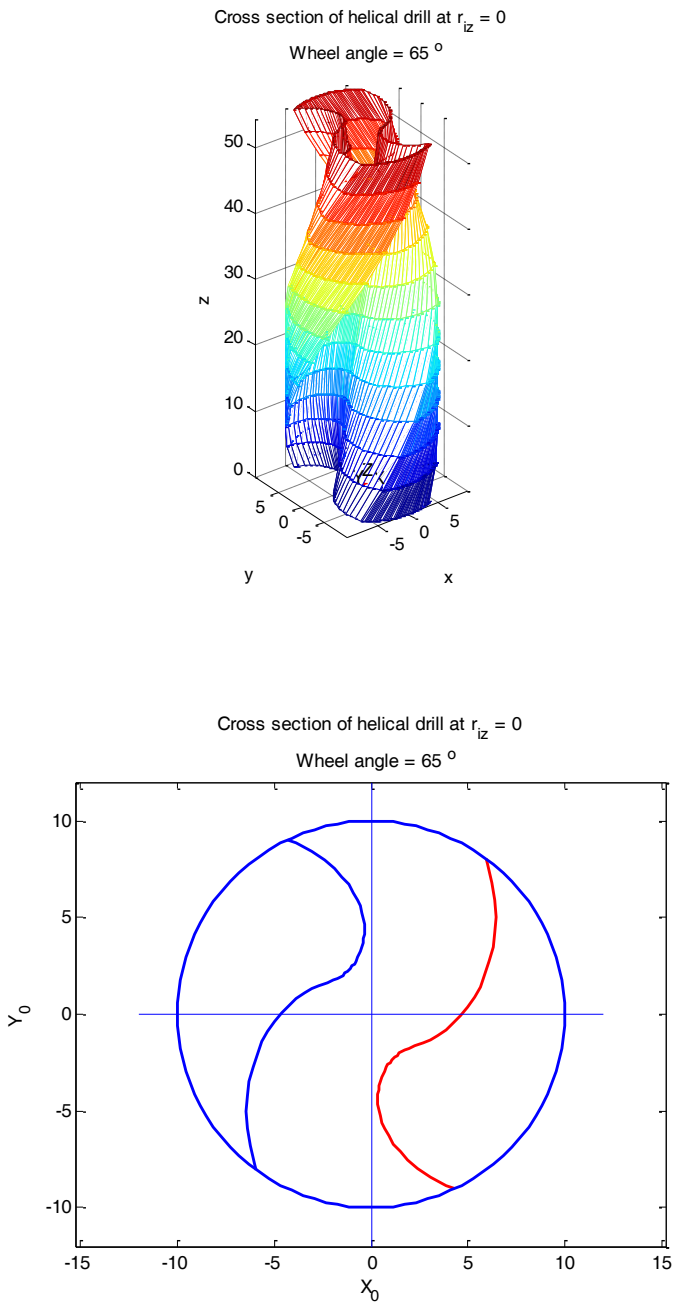

Figure 3-7 The three-dimensional flute and its cross section of the drill machined using the No. 3 grinding wheel.

3.3 Inverse Method of Machining Flutes

In the tool manufacturing industry, sometimes cutters are designed with the flute

cross-sectional profiles, and the manufacturing tolerances of the flutes are high. To accurately make the flutes, the direct method of machining flutes using standard grinding wheels cannot realize this goal; thus, the inverse method is necessary. The inverse method of machining flutes is to compute the grinding wheel profile based on the flute design, make a non-standard wheel with the calculated profile, and grind the flute with a set of appropriate cutting parameters, in order to achieve high flute accuracy. The kernel technique of finding the wheel profile is the conjugate theory between the virtual grinding wheel and the designed flute. This method is introduced in the following.

3.3.1 Formula of the Flute Surface and its Normal

In general, a flute surface is a curve (or multiple curves) on the cutter cross section sweeping along the cutting edge. A flute surface is shown in Fig. 3.9. In this work, a cutter coordinate system $(x_d y_d z_d)$ is established in a way that the z_d axis is along the cutter axis from the bottom to the top and the x_d and the y_d axes are on the cross section. Here, a generic mathematical representation of the desired flute surface $\mathbf{F}_d(r,v)$ in the cutter coordinate system is adopted as

$$\mathbf{F}_d(r,v)=\begin{bmatrix} \mathrm{Fx}_d(r,v) \\ \mathrm{Fy}_d(r,v) \\ \mathrm{Fz}_d(r,v) \end{bmatrix}, \tag{3.21}$$

where the parameter r represents the radial variable and the parameter v represents the rotating variable. So the equation of the normal vector $\mathbf{N}_d(r,v)$ of the flute surface is

$$\mathbf{N}_d(r,v)=\begin{bmatrix}\mathrm{Nx}_d(r,v)\\ \mathrm{Ny}_d(r,v)\\ \mathrm{Nz}_d(r,v)\end{bmatrix}=\frac{\partial \mathbf{N}_d}{\partial r}\times\frac{\partial \mathbf{N}_d}{\partial v}=\begin{vmatrix} i & j & k\\ \dfrac{\partial \mathrm{Fx}_d}{\partial r} & \dfrac{\partial \mathrm{Fy}_d}{\partial r} & \dfrac{\partial \mathrm{Fz}_d}{\partial r}\\ \dfrac{\partial \mathrm{Fx}_d}{\partial v} & \dfrac{\partial \mathrm{Fy}_d}{\partial v} & \dfrac{\partial \mathrm{Fz}_d}{\partial v}\end{vmatrix}. \qquad (3.22)$$

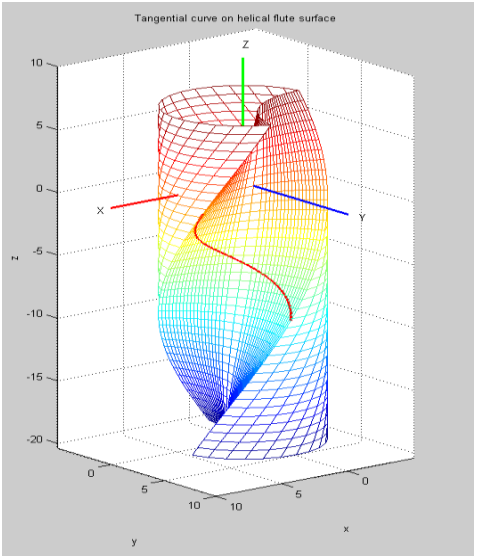

Figure 3-8 A contact curve of the flute surface shown with the grinding wheel not shown.

3.3.2 Conjugate Relationship between the Flute and the Wheel

In the reverse method of machining the flutes, the wheel profile is to be determined (see Fig. 3-9), while, at beginning, the wheel coordinate system $(x_g y_g z_g)$ is defined with the x_g axis in line with the wheel axis. According to the kinematics of the multi-axis CNC grinding of flutes, the wheel, together with its coordinate system, can be represented in the cutter coordinate system $(x_d y_d z_d)$. For this purpose, it is assumed that the grinding wheel coordinate system $(x_g y_g z_g)$ is coincided with the cutter coordinate system $(x_d y_d z_d)$ before grinding. During machining, the rotation angle θ of the cutter changes, and the wheel location and orientation change accordingly. The specific

steps are provided in the following.

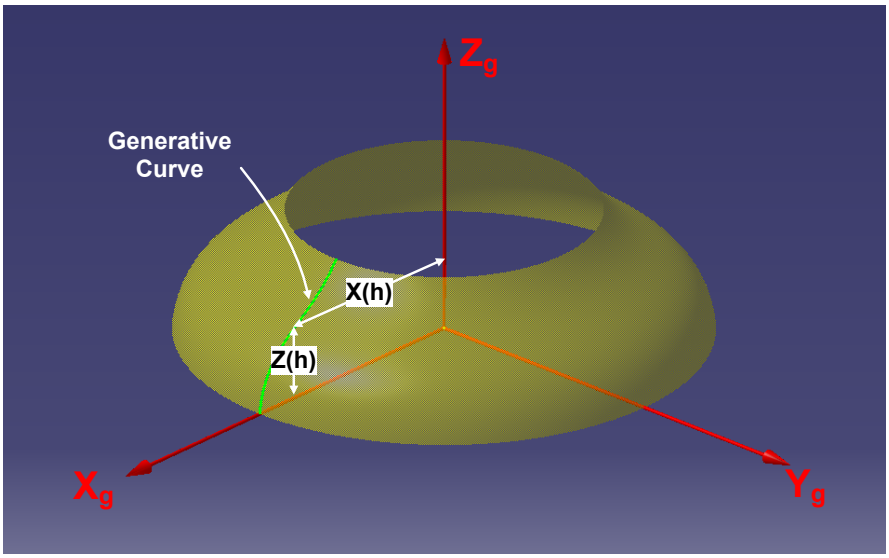

Figure 3-9 The profile of a non-standard grinding wheel.

The wheel coordinate system is rotated about its z_g axis by θ. The rotation matrix is $\mathbf{M}^{\mathrm{R}}\left(z_g,\theta\right)=\begin{bmatrix}\cos\theta & -\sin\theta & 0 & 0\\ \sin\theta & \cos\theta & 0 & 0\\ 0 & 0 & 1 & 0\\ 0 & 0 & 0 & 1\end{bmatrix}$.

The wheel coordinate system is translated along its x_g axis by Δx_g, which is equal to $\left(\mathrm{R_w}+r_c\right)+k_x\cdot\theta$. k_x is related with the taper angle of the cutter. The translation matrix is $\mathbf{M}^{\mathrm{T}}\left(\Delta x_g,0,0\right)=\begin{bmatrix}1 & 0 & 0 & \Delta x_g\\ 0 & 1 & 0 & 0\\ 0 & 0 & 1 & 0\\ 0 & 0 & 0 & 1\end{bmatrix}$.

The wheel coordinate system is rotated about its x_g axis by angle β. The rotation matrix is $\mathbf{M}^{\mathrm{R}}\left(x_g,\theta\right)=\begin{bmatrix}1 & 0 & 0 & 0\\ \cos\theta & -\sin\theta & 0 & 0\\ \sin\theta & \cos\theta & 0 & 0\\ 0 & 0 & 0 & 1\end{bmatrix}$.

The wheel coordinate system is rotated about its y_g axis by angle α. The

rotation matrix is $\mathbf{M}^{\mathrm{R}}\left(y_g,\theta\right)=\begin{bmatrix}\cos\theta & 0 & \sin\theta & 0\\ 0 & 1 & 0 & 0\\ -\sin\theta & 0 & \cos\theta & 0\\ 0 & 0 & 0 & 1\end{bmatrix}$.

Using the Euler rule, the equivalent matrix of the four transformation matrices can be derived as

$$
\begin{aligned}
{}^{d}_{g}\mathbf{M}\left(\theta,\alpha,\beta,k_x,k_z\right)&=\mathbf{M}^{\mathrm{R}}\left(z_g,\theta\right)\cdot\mathbf{M}^{\mathrm{T}}\left(\Delta x_g,0,0\right)\cdot\mathbf{M}^{\mathrm{R}}\left(x_g,\beta\right)\cdot\mathbf{M}^{\mathrm{R}}\left(y_g,\alpha\right)\\
&=\begin{bmatrix}\cos\theta\cdot\cos\alpha-\sin\theta\cdot\sin\beta\cdot\sin\alpha & -\sin\theta\cdot\cos\beta & \cos\theta\cdot\sin\alpha+\sin\theta\cdot\sin\beta\cdot\cos\alpha & \Delta x_g\cdot\cos\theta\\ \sin\theta\cdot\cos\alpha+\cos\theta\cdot\sin\beta\cdot\sin\alpha & \cos\theta\cdot\cos\beta & \sin\theta\cdot\sin\alpha-\cos\theta\cdot\sin\beta\cdot\cos\alpha & \Delta x_g\cdot\sin\theta\\ -\cos\beta\cdot\sin\alpha & \sin\beta & \cos\beta\cdot\cos\alpha & 0\\ 0 & 0 & 0 & 1\end{bmatrix}\cdot
\end{aligned}
\tag{3.23}
$$

A point on the z_g axis is represented as $\mathbf{z}_g\left(\lambda_1\right)=\begin{bmatrix}0 & 0 & \lambda_1\end{bmatrix}^{\mathrm{T}}$ in the wheel coordinate system, and it can be represented in the cutter coordinate system as

$$
\begin{bmatrix}{}^{d}\mathbf{z}_g\left(\lambda_1\right)\\ 1\end{bmatrix}={}^{d}_{g}\mathbf{M}\left(\theta,\alpha,\beta,k_x,k_z\right)\cdot\begin{bmatrix}\mathbf{z}_g\left(\lambda_1\right)\\ 1\end{bmatrix}=\begin{bmatrix}\lambda_1\cdot b_1+c_1\\ \lambda_1\cdot b_2+c_2\\ \lambda_1\cdot b_3+c_3\\ 1\end{bmatrix},
\tag{3.24}
$$

where

$b_1=\cos\theta\cdot\sin\alpha+\sin\theta\cdot\sin\beta\cdot\cos\alpha$, $b_2=\sin\theta\cdot\sin\alpha-\cos\theta\cdot\sin\beta\cdot\cos\alpha$, $b_3=\cos\beta\cdot\cos\alpha$, $c_1=\Delta x_g\cdot\cos\theta$, $c_2=\Delta x_g\cdot\sin\theta$, and $c_3=0$.

During machining, the wheel contacts with the flute at an effective grinding edge, thus, they are conjugate with each other. According to the conjugate theory, at the points where the wheel contacts with the flute surface during machining, the normals to

the two surfaces are in line. Since the wheel surface is a revolving surface, a normal to the wheel surface passes through the wheel axis. Therefore, for the flute points, the normals to the designed flute surface at these points pass through the wheel axis. The conjugate relationship can be formulated in the cutter coordinate system so that the contact curve on the flute surface or the effective grinding edge can be found. The intersection point between a normal to the designed flute surface at the contact point and the wheel axis can be represented as

$$\mathbf{F}_d(r,v)+\lambda_2\cdot\mathbf{N}_d(r,v)=\begin{bmatrix}\mathrm{Fx}_d(r,v)+\lambda_2\cdot\mathrm{Nx}_d(r,v)\\ \mathrm{Fy}_d(r,v)+\lambda_2\cdot\mathrm{Ny}_d(r,v)\\ \mathrm{Fz}_d(r,v)+\lambda_2\cdot\mathrm{Nz}_d(r,v)\end{bmatrix}, \tag{3.25}$$

Where λ_2 is distance between the contact point and the intersection point. Then, the equation of the conjugate relationship is

$${}^{d}\mathbf{z}_g=\mathbf{F}_d(r,v)+\lambda_2\cdot\mathbf{N}_d(r,v). \tag{3.26}$$

This equation can be represented in the scale form as

$$\begin{bmatrix}\lambda_1\cdot b_1+c_1\\ \lambda_1\cdot b_2+c_2\\ \lambda_1\cdot b_3+c_3\end{bmatrix}=\begin{bmatrix}\mathrm{Fx}_d(r,v)+\lambda_2\cdot\mathrm{Nx}_d(r,v)\\ \mathrm{Fy}_d(r,v)+\lambda_2\cdot\mathrm{Ny}_d(r,v)\\ \mathrm{Fz}_d(r,v)+\lambda_2\cdot\mathrm{Nz}_d(r,v)\end{bmatrix}. \tag{3.27}$$

Solving the above equations by eliminating λ_1 and λ_2, the following equation can be derived.

$$\frac{\mathrm{Nx}_d\cdot(\mathrm{Fz}_d-c_3)-\mathrm{Nz}_d\cdot(\mathrm{Fy}_d-c_2)}{b_3\cdot\mathrm{Ny}_d-b_2\cdot\mathrm{Nz}_d}\cdot b_1+c_1=\mathrm{Fx}_d+\frac{b_2\cdot(\mathrm{Fz}_d-c_3)-b_3\cdot(\mathrm{Fy}_d-c_2)}{b_3\cdot\mathrm{Ny}_d-b_2\cdot\mathrm{Nz}_d}\cdot\mathrm{Nx}_d. \tag{3.28}$$

With this equation, the relationship between the two parameters, *r* and *v*, is

attained, and the contact curve on the flute surface can be found, which can be represented as

$$\mathbf{C}_d = \begin{bmatrix} \mathrm{Fx}_d\left(r, v(r)\right) \\ \mathrm{Fy}_d\left(r, v(r)\right) \\ \mathrm{Fz}_d\left(r, v(r)\right) \end{bmatrix}. \tag{3.29}$$

3.3.3 Grinding Wheel Profile

The main objective of the inverse method is to find the grinding wheel profile so that a non-standard grinding wheel can be made for machining the designed flute. The contact curve has been found in the above section in the cutter coordinate system. Since the contact curve on the flute surface and the effective grinding edge on the wheel surface are the same, the equation of the effective grinding edge in the wheel coordinate system can be found by using the inverse kinematics of the flute machining. Based on Eq. 3.22 of the kinematics of the flute machining, the equation of the inverse kinematics is

$$\begin{aligned} {}^{d}_{g}\mathbf{M}\left(\theta,\alpha,\beta,k_x,k_z\right) &= \mathbf{M}^{\mathrm{R}}\left(y_g,-\alpha\right)\cdot\mathbf{M}^{\mathrm{R}}\left(x_g,-\beta\right)\cdot\mathbf{M}^{\mathrm{T}}\left(-\Delta x_g,0,0\right)\cdot\mathbf{M}^{\mathrm{R}}\left(z_g,-\theta\right) \\ &= \begin{bmatrix} \cos\theta\cdot\cos\alpha-\sin\theta\cdot\sin\beta\cdot\sin\alpha & \sin\theta\cdot\cos\alpha+\cos\theta\cdot\sin\beta\cdot\sin\alpha & -\cos\beta\cdot\sin\alpha & -\Delta x_g\cdot\cos\alpha \\ -\sin\theta\cdot\cos\beta & \cos\theta\cdot\cos\beta & \sin\beta & 0 \\ \cos\theta\cdot\sin\alpha+\sin\theta\cdot\sin\beta\cdot\cos\alpha & \sin\theta\cdot\sin\alpha-\cos\theta\cdot\sin\beta\cdot\cos\alpha & \cos\beta\cdot\cos\alpha & -\Delta x_g\cdot\sin\alpha \\ 0 & 0 & 0 & 1 \end{bmatrix}. \end{aligned} \tag{3.30}$$

Therefore, the effective grinding edge can be found as

$$\mathbf{E}_g = \begin{bmatrix} \mathrm{Ex}_g\left(r\right) \\ \mathrm{Ey}_g\left(r\right) \\ \mathrm{Ez}_g\left(r\right) \end{bmatrix} = {}^{g}_{d}\mathbf{M}\cdot\mathbf{C}_d. \tag{3.31}$$

The wheel surface can be expressed as

$$\mathbf{W}_g(r,\phi)=\begin{bmatrix} \mathrm{Wx}_g(r,\phi) \\ \mathrm{Wy}_g(r,\phi) \\ \mathrm{Wz}_g(r,\phi) \end{bmatrix}=\begin{bmatrix} \sqrt{\left(\mathrm{Ex}_g(r)\right)^2+\left(\mathrm{Ey}_g(r)\right)^2}\cdot\cos\phi \\ \sqrt{\left(\mathrm{Ex}_g(r)\right)^2+\left(\mathrm{Ey}_g(r)\right)^2}\cdot\sin\phi \\ \mathrm{Ez}_g(r) \end{bmatrix}. \tag{3.32}$$

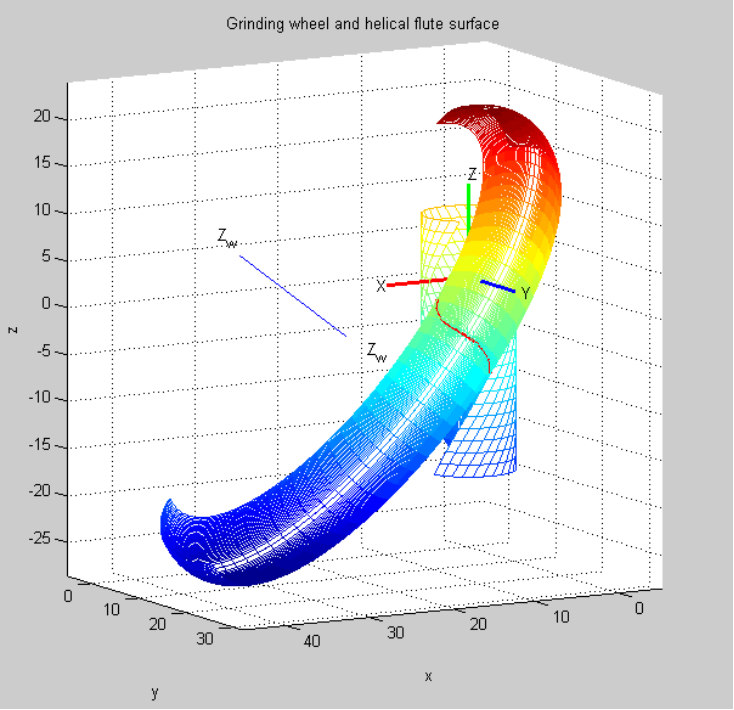

Figure 3-10 The effective grinding edge of the virtual grinding wheel.

3.3.4 Grinding Wheel Profile

Based on the representation of the wheel surface in the wheel coordinate system, the wheel profile is the intersection curve between the wheel surface and the principle plane $x_g z_g$. Thus, the grinding wheel profile can be formulated as

$$\mathbf{P}_g(r)=\begin{bmatrix} Px_g(r) \\ Py_g(r) \\ Pz_g(r) \end{bmatrix}=\begin{bmatrix} \sqrt{\left(\mathrm{Ex}_g(r)\right)^2+\left(\mathrm{Ey}_g(r)\right)^2} \\ 0 \\ \mathrm{Ez}_g(r) \end{bmatrix}. \tag{3.33}$$

3.3.5 Applications of the Inverse Method

The inverse method of grinding flutes is provided in the above sections. To show its validity, the inverse method is now applied to three examples. In the first example, a drill is designed; its diameter is 10 mm, its web thickness is 2 mm (or the core radius is 1 mm), the point angle is 140 degrees, the helix angle of the flute is 30 degrees. The maximum grinding wheel radius is specified as 29 mm. The cross sectional profile of the flute is provided. By using the inverse method, the contact curve between the wheel and the given flute is first found; the curve actually is the effective grinding edge of the wheel. Then, the cross sectional profile of the wheel is determined. As results, they are plotted in the following diagrams.

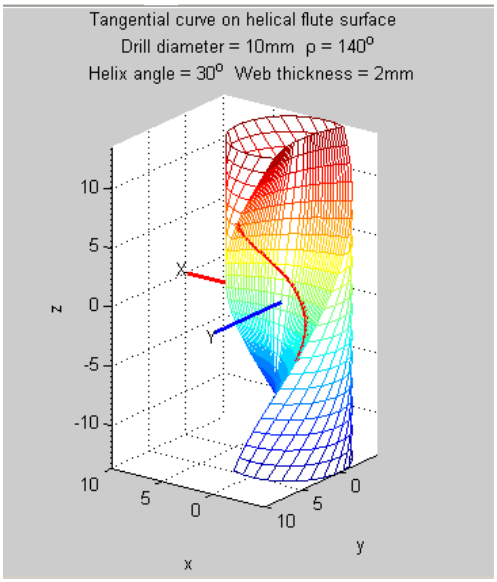

Figure 3-11 A contact curve between the flute surface shown and the grinding wheel not shown in the first example.

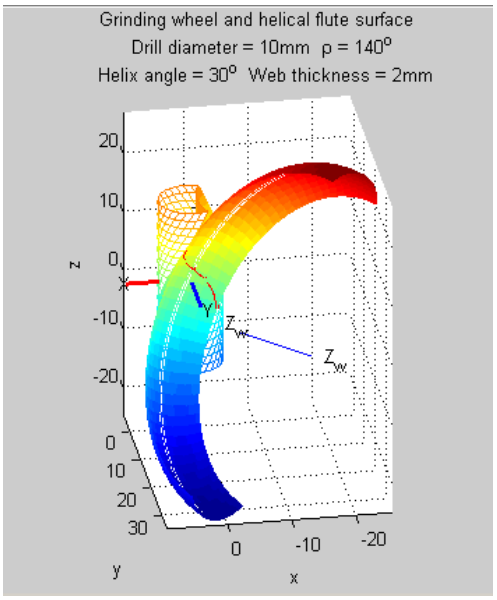

Figure 3-12 The effective grinding edge of the wheel in the first example.

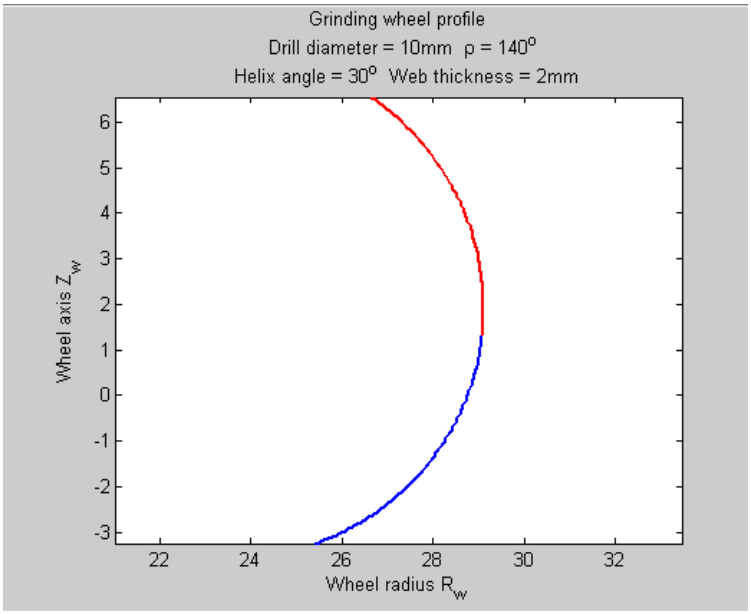

Figure 3-13 The cross sectional profile of the wheel in the first example.

In the second example, the same drill as that in the first example, except the point

angle is 120 degrees. The grinding wheel radius is 39 mm, which is larger than the wheel in the first example. Similarly, the inverse method is applied, and the contact curve between the wheel and the given flute (or the effective grinding edge of the wheel) and the cross sectional profile of the wheel are found. Here, they are shown in the following diagrams.

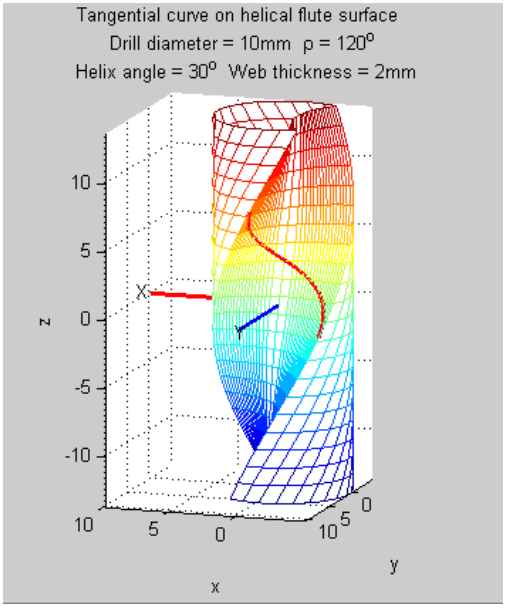

Figure 3-14 A contact curve between the flute surface shown and the grinding wheel not shown in the second example.

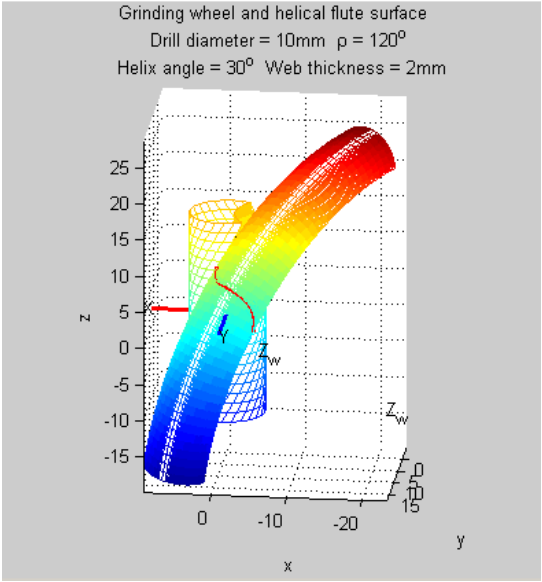

Figure 3-15 The effective grinding edge on the wheel in the second example.

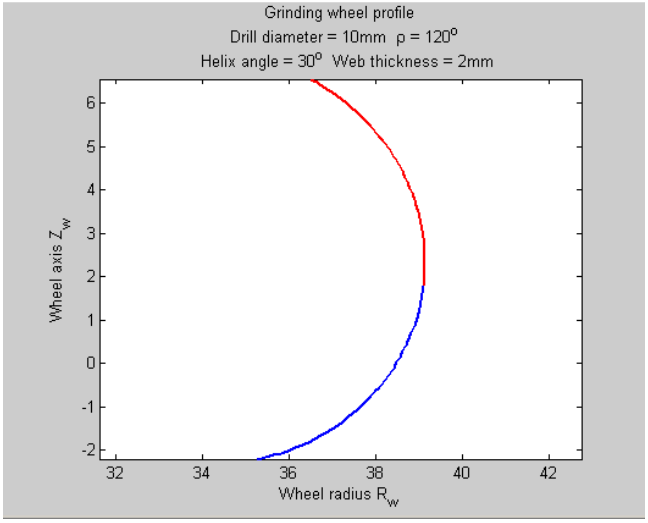

Figure 3-16 The cross sectional profile of the wheel in the second example.

In the third example, the drill is the same as that in the first example, except the point angle is 140 degrees in this example. The grinding wheel used in this example is 59 mm in radius, which is twice as large as that in the first example. After the inverse method is applied, and the contact curve between the wheel and the given flute (or

effective grinding edge of the wheel) and the cross sectional profile of the wheel are found. Here, they are shown in the following diagrams.

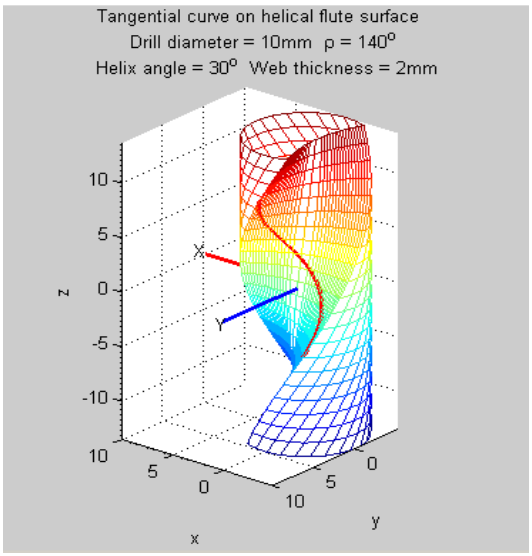

Figure 3-17 A contact curve between the flute surface shown and the grinding wheel not shown in the third example.

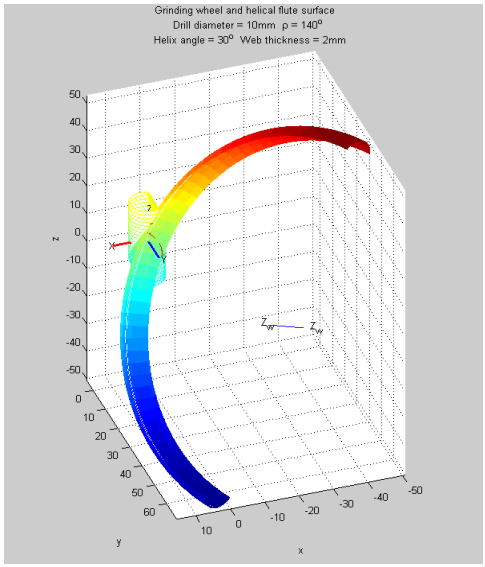

Figure 3-18 The effective grinding edge on the wheel in the third example.

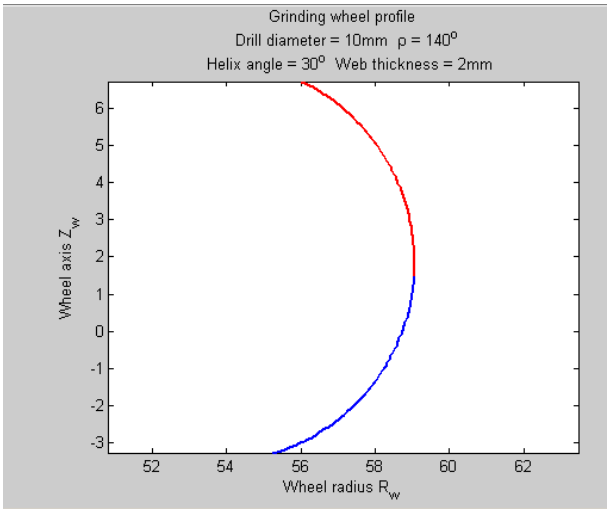

Figure 3-19 The cross sectional profile of the wheel in the third example.

With the profile of the grinding wheel determined, a corresponding grinding wheel can be made. Then it can be used to grind the designed flute with high accuracy. The next steps are the same as the steps in the direct method, and they are not elaborated here.

3.4 Example of Geometrically Modeling of the Flutes

Based on the above analysis, several MATLAB programs are designed for finding the points on the effective grinding edge by a standard straight wheel. The data of the points is then input to the CATIA. Using B-spline curves to connect these points, the effective grinding edges are then built in CATIA . Sweeping these EGEs, along with the grinding wheel position, the flute surface is finally created in CATIA accurately.

The parameters used in programming and geometrically modeling are list below.

Table 3-2 Parameters in flute modeling and programming

Drill diameter (mm)	Core diameter (web thickness) (mm)	Grinding wheel diameter (mm)	Helix angle β (°)	Wheel inclination angle α (°)
12	3	150	30	25

3.4.1 Effective grinding edge obtained by MATLAB programming

Figure 3-20 shows the effective grinding edges (EGEs) generated by a parallel grinding wheel. The red curves are generated by the corner and the cylindrical surface of the grinding wheel. The straight blue line is by the wheel side surface.

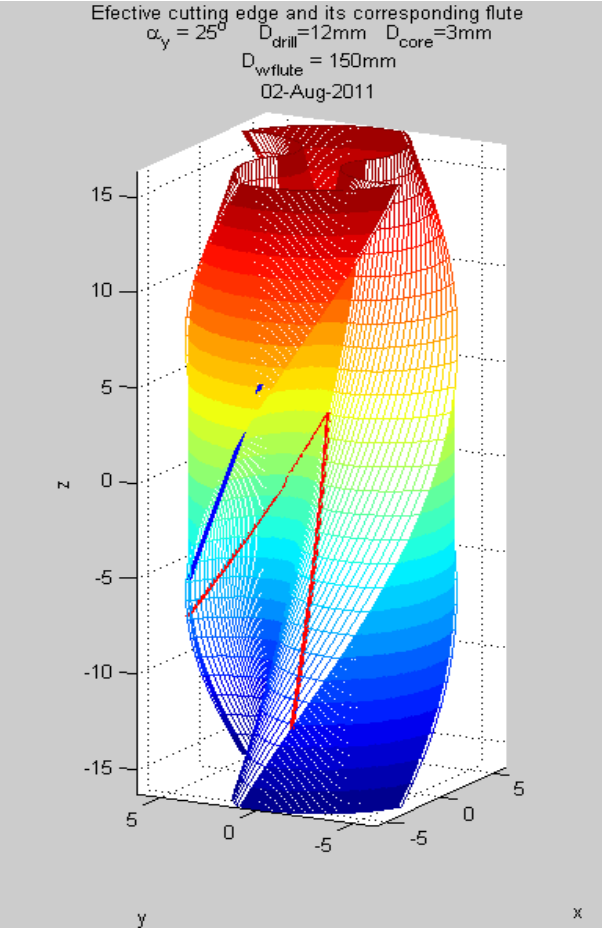

Figure 3-20 Effective grinding edge generated by a parallel grinding wheel.

3.4.2 Input to CATIA

Figure 3-21 shows the EGE (red color) in 3-D CATIA model. The white points are input from the data calculated by programming. The red EGE sweeps along the drill's helical curve, whose color is yellow, and forms the main flute, which is also an envelope surface.

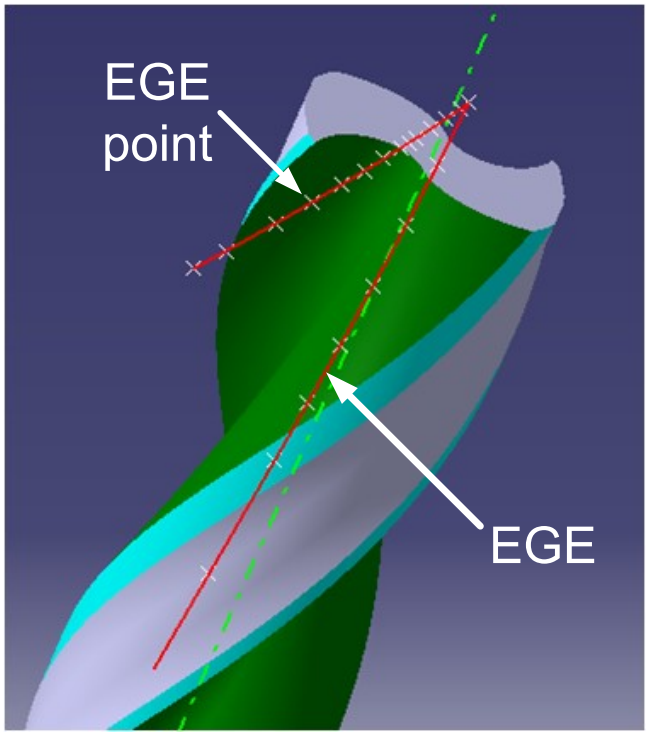

Figure 3-21 EGE in CATIA

The yellow curve in Figure 3-22 is a helical curve with the lead same as the drill helical flute.

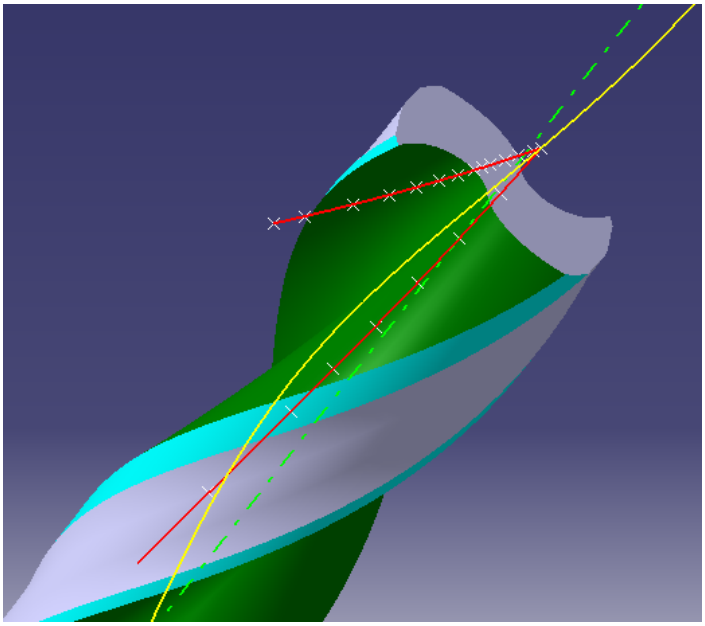

Figure 3-22 EGE and helical curve

Figure 3-23 shows the EGEs at different positions. The envelope surface is formed by sweeping the EGE along the helix curve of the drill.

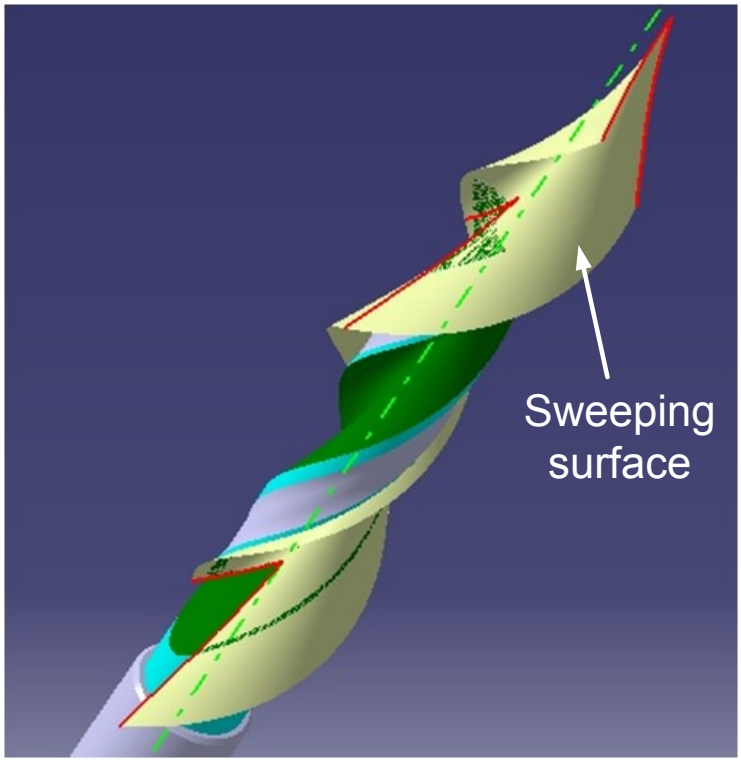

Figure 3-23 The envelope surface swept by EGE

To get the final flute, we need to consider the surface of the grinding wheel at final position. Here, the kinematics of the grinding process is also built in 3-D model. The movement of the grinding wheel coordinate system is shown in Figure 3-24 to Figure 3-28.

First step, as shown in Figure 3-24, the wheel coordinate system coincides with the drill coordinated system (the orange color) and then translates along its axis z_g to a new position (blue color) by the flute length Δz_g (here = 60 mm).

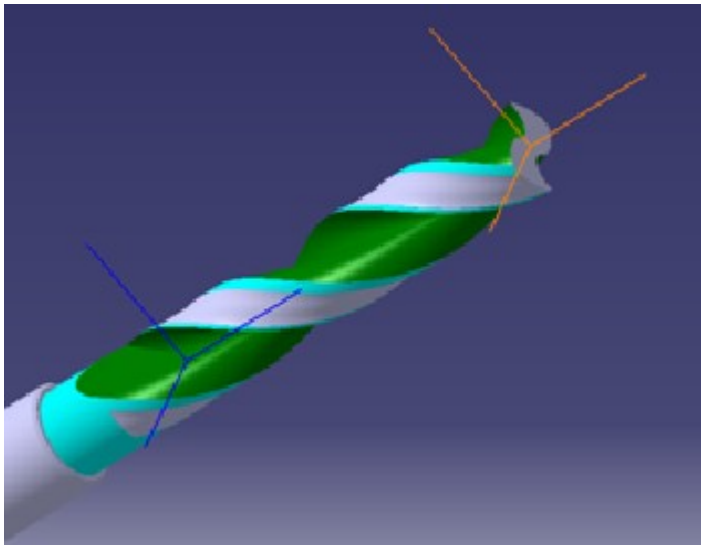

Figure 3-24 Flute modeling: Step 1

Second, the blue coordinate system rotates about its z-axis by θ as shown in Fig 3-25. The new wheel coordinate system is shown in red. The relationship between the flute length and the angle is

$$\theta = \frac{\Delta z_g \cdot \tan(\beta)}{\pi \cdot D_{drill}} \cdot 360 \quad \text{(degree).}$$

Substituting the values of the flute length Δz_g, the helix angle β, and the drill diameter D_{drill}, the value of ϑ is obtained as

$$\theta = \frac{-60mm \cdot \tan(30°)}{\pi \cdot 12mm} \cdot 360°$$
$$= -328.063°$$

.

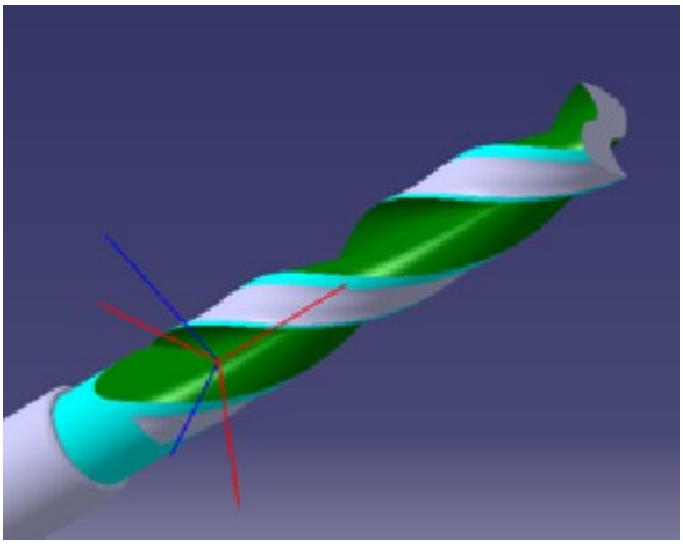

Figure 3-25 Flute modeling: Step 2

Third, the red coordinate system rotates about its x-axis by angle λ as shown in Figure 3-26. The new coordinate system is shown in white. Normally, the angle λ is set to around $(\lambda = 90° - \beta)$ so that the wheel orientation corresponds the helix direction.

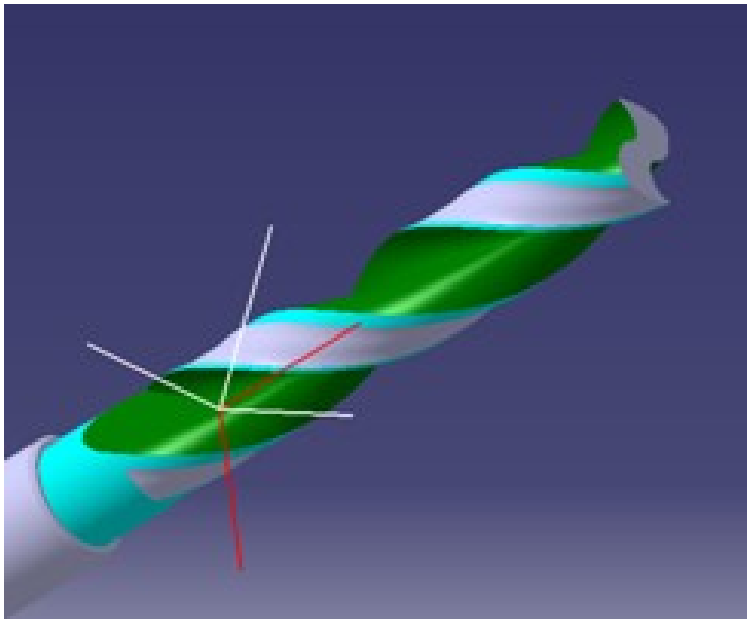

Figure 3-26 Flute modeling: Step 3

Fourth, the wheel coordinate system (white) rotates about its y-axis by α. The new wheel coordinate system is shown in yellow (Figure 3-27).

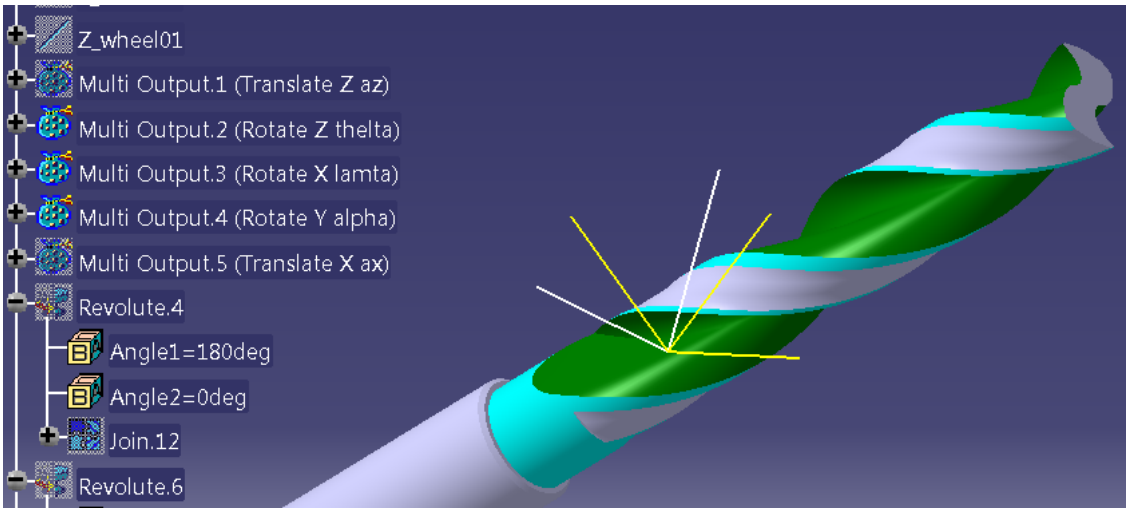

Figure 3-27 Flute modeling: Step 4

Finally, the yellow coordinate system translates along its x-axis by Δx_g . the new one is shown in red (Figure 3-28). This final coordinate system (red) defines the wheel's final position and orientation. The Δx_g is calculated according to the following formula

$$\Delta x_g = \frac{D_{wheel}}{2} + \frac{D_{core}}{2} \cdot \frac{1}{\cos\alpha}$$

Substituting the values of the grinding wheel diameter D_{wheel}, the core diameter D_{core}, and the angle α, the value of Δx_g is

$$\Delta x_g = \frac{150mm}{2} + \frac{3mm}{2} \cdot \frac{1}{\cos 25°}$$
$$= 76.746(mm)$$

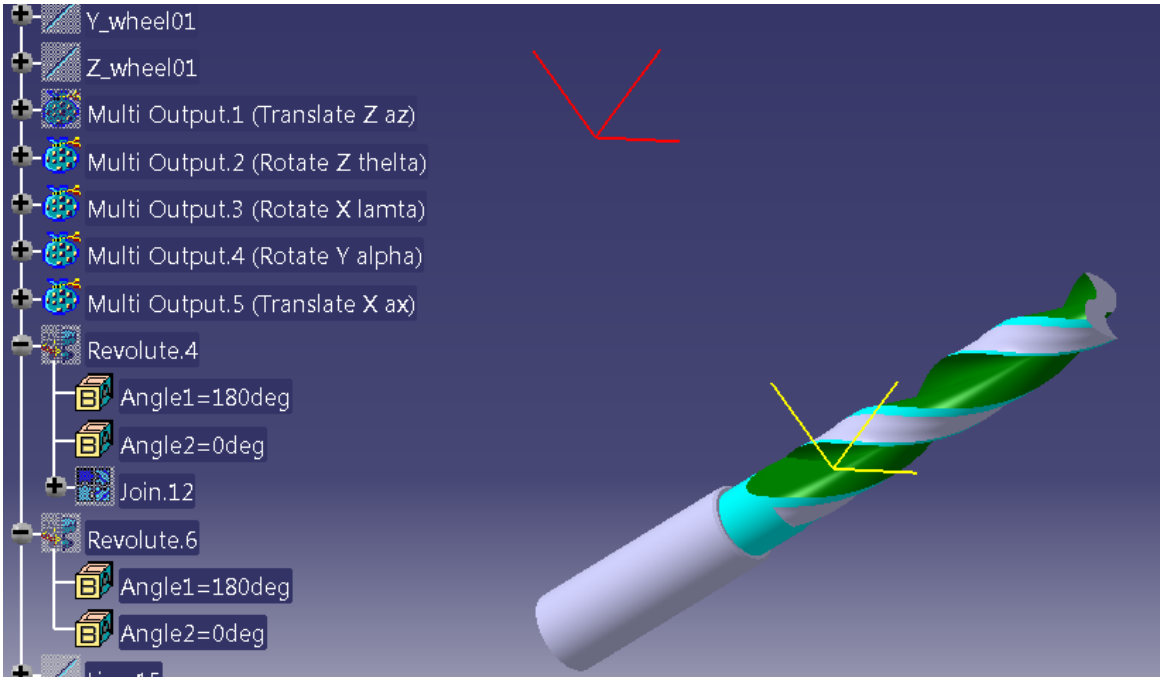

Figure 3-28 Flute modeling: Step 5

Since the connection area of the end of the flute and the drill body is formed by a pure wheel surface, we need to draw a wheel at its final position. Figure 3-29 draws the grinding wheel at its final position.

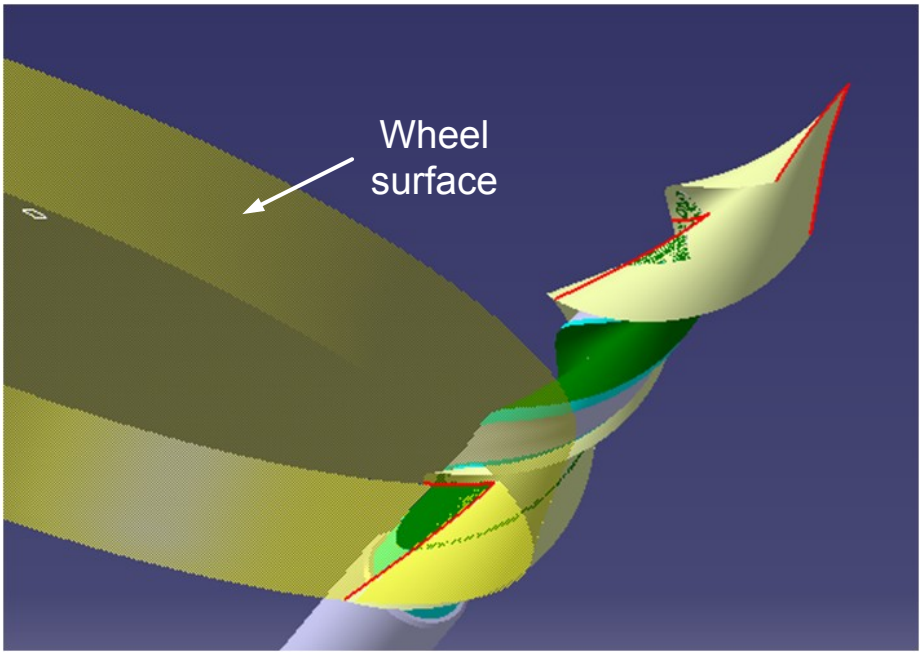

Figure 3-29 Flute modeling: Step 6, adding wheel surface at final position

Adding the final wheel surface, as shown in Figure 3-29, to the envelope surface obtained before, and doing a split operation (splitting the volume from the drill body by the envelope surface and the final grinding wheel surface), the final flute (green) is then obtained in Figure 3-30.

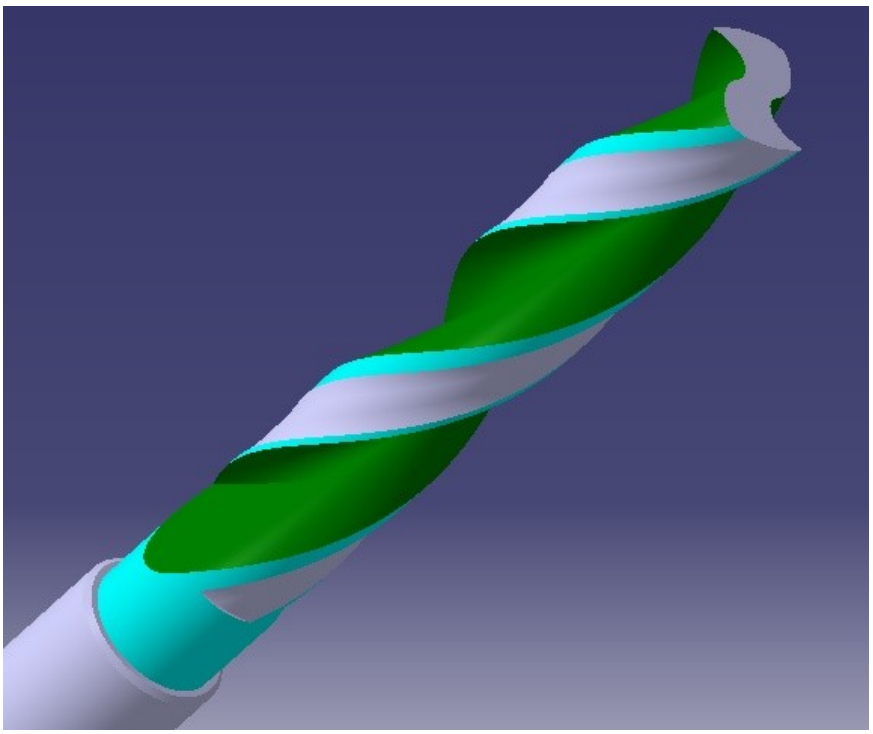

Figure 3-30 Flute modeling: Step 7, create final flute shape

Chapter 4 Flank Modeling

In general, the geometry of a twist drill tip includes the flank faces and the chisel edge, which is the intersection curve between the flank faces. Since some drills have gashes and some do not, the gash is regarded as a different feature, which will be discussed in the following section. The drill tip is a feature that significantly affects the drill performance and life, so it is crucial to correctly construct the drill tip geometry in the solid model of the cutter. Currently, the drill tip flanks are classified into four main types according to their shapes, planar, quadratic, helical, and multi-facet flanks. The planar flanks include single plane flanks and multi-plane flanks; the quadratic flanks include conical, cylindrical, ellipsoidal (Racon), and hyperboloidal flanks; the helical flanks include constant and non-constant helix angle flanks; and the multi-facet flanks are special flanks which combines multi-type flanks in one point. Different flanks are made with different manufacturing methods. Since the flank faces determine the cutting edge shape, the drill point angle, and the relief angle, it is very important to model the manufacturing methods in order to build the solid flank models in accordance to the actual flanks. Eventually, the chisel edge is found automatically as the intersection between the flanks. Therefore, parametric modeling of the twist drill flank is vital to drill simulation.

Since the planar model is simple, this work will discuss the mathematical models mainly for a popular quadratic flank, conical flank. The geometric models will be built for conical and planar flank.

4.1 Mathematical models of the flank

4.1.1 Mathematical model for the quadratic flanks

The general mathematical model of the quadratic flanks is

$$\frac{x_g^{\,2}}{a^2}+\frac{y_g^{\,2}}{a^2}+\delta\frac{z_g^{\,2}}{c^2}=0 \tag{4.1}$$

where,

for conical flank, $\delta=-1$, $a\to 0$, $c\to 0$ and set $\tan\theta=\frac{a}{c}$;

for hyperboloidal flank, $\delta=-1$;

for ellipsoidal flank, $\delta=1$;

and for cylindrical flank, $\delta=0$.

Specially, for conical flank the points in cone coordinate system has the following relationship

$$x_g^{\,2}+y_g^{\,2}-\left(z_g\cdot\tan\theta\right)^2=0 \tag{4.2}$$

The point on conical flank in drill coordinate system has the following relationship

$$\begin{aligned}&\left(\left(x_d\cos\omega+y_d\sin\omega\right)-S\right)^2\\&+\left(\left(-x_d\sin\omega+y_d\cos\omega\right)\cos\phi-z_d\sin\phi-\sqrt{\left(d\tan\theta\right)^2-S^2}\right)^2\\&-\tan^2\theta\left(\left(-x_d\sin\omega+y_d\cos\omega\right)\sin\varphi+z_d\cos\varphi-d\right)^2=0\end{aligned}\tag{4.3}$$

The detailed processes to derive this equation will be shown in section 4.3, 'Parametric modeling of the conical flanks of the drill tip'.

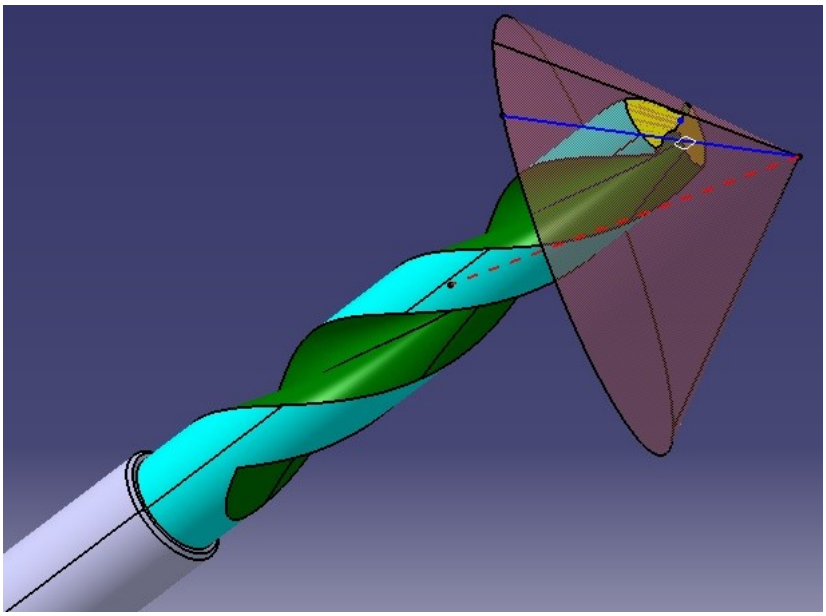

Figure 4-1 Conical flank and grinding cone

4.1.2 Mathematical model for the planar flanks

Another popular drill point has planar flank. The grinding wheel coordinate system coincides with the drill system at the beginning. Following a series translation and rotations, the wheel end face gets to the flank position and be able to work out the flank

face.

The transformation matrix is

$$ {}^{d}_{g}\mathbf{T} = Trans(s,0,0)Rot(x,\pi/2-\rho)Rot(y,\alpha) $$

The transformation and rotations are shown in the parametric modeling section. From the transformation matrix, the mathematical model of planar flank is

$$ \begin{aligned} {}^{d}\mathbf{S}(u,v) &= {}^{d}_{g}\mathbf{T}\,{}^{g}\mathbf{S}(u,v) \\ &= \begin{bmatrix} \cos\alpha & 0 & \cos\alpha & s \\ \cos\rho\sin\alpha & \sin\rho & -\cos\rho\cos\alpha & 0 \\ -\sin\rho\sin\alpha & \cos\rho & \sin\rho\cos\alpha & 0 \\ 0 & 0 & 0 & 1 \end{bmatrix} \begin{bmatrix} u \\ v \\ 0 \\ 1 \end{bmatrix} \\ &= \begin{bmatrix} s+u\cos\alpha \\ u\cos\rho\sin\alpha+v\sin\rho \\ -u\sin\rho\sin\alpha+v\cos\rho \\ 1 \end{bmatrix} \end{aligned} \tag{4.4} $$

4.2 Parametric modeling of the conical flanks of the drill tip

To build the parametric model of the conical flanks of the twist drill tip, the 'half point angel', 'half cone angle', 'distance from the cone vertex to drill tip', 'skew distance from drill axis to cone axis', and 'chisel edge angle' are taken as the parameters.

Table 4-1 Parameters for conical flank modeling

Parameters	Definition	value
ρ	Drill half point angle	70 °

θ	Half cone angle	45 ^{o}
d	Distance from the cone vertex to drill tip measuring along the cone axis	10 mm
S	Skew distance between the drill axis and the cone axis	3 mm
ζ	Chisel edge angle	100 ^{o}

After the grinding wheel is properly oriented, a conical flank can be grinded with the side of the wheel in a path.

First, the cone coordinate system coincides with the drill coordinate system.

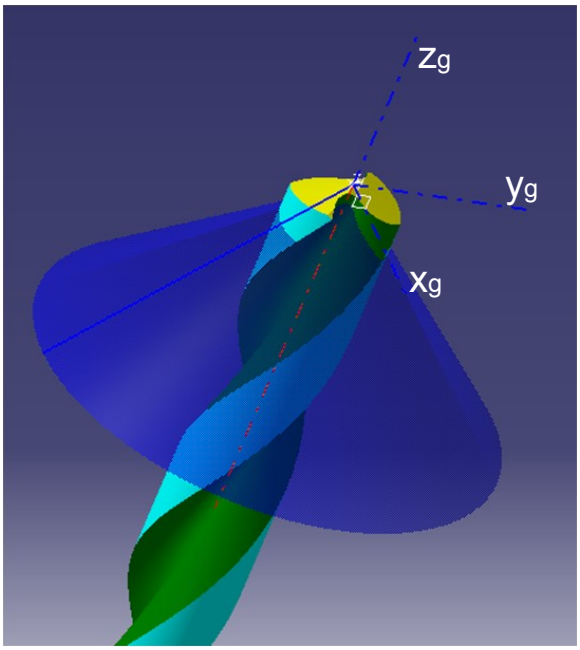

Figure 4-2 Conical flank modeling: Step 1

Second, the cone and its coordinate system rotates about its x-axis about $-\phi$.

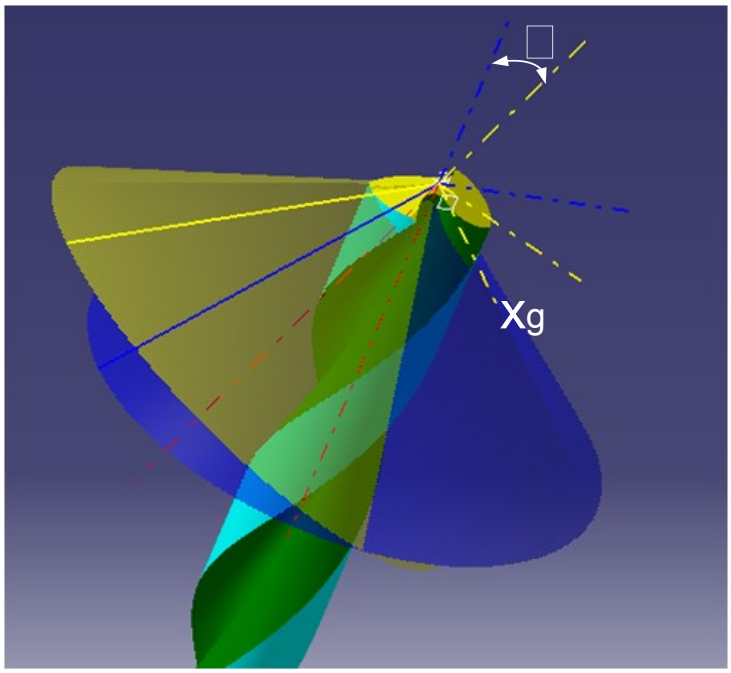

Figure 4-3 Conical flank modeling: Step 2

Third, the cone and its coordinate system translates along its z-axis with *d*.

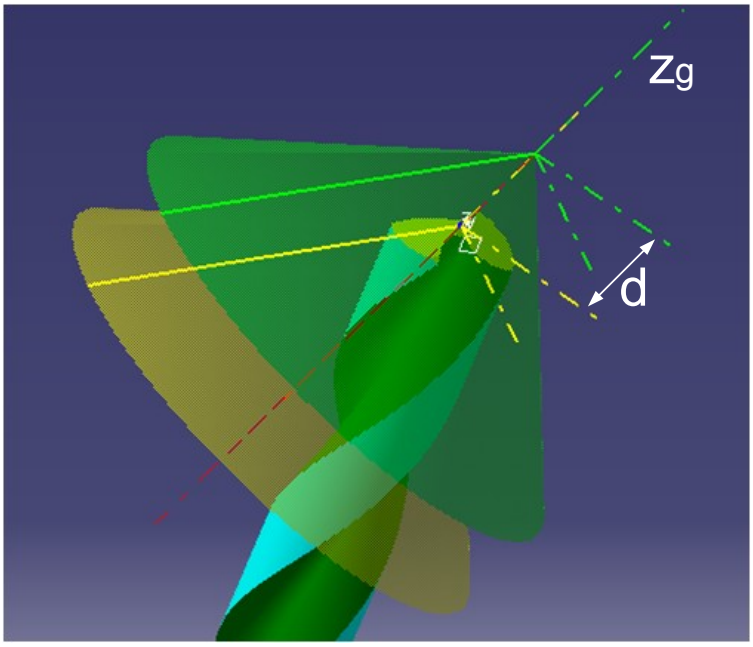

Figure 4-4 Conical flank modeling: Step 3

Fourth, the cone and its coordinate system translates along its x-axis with *S*.

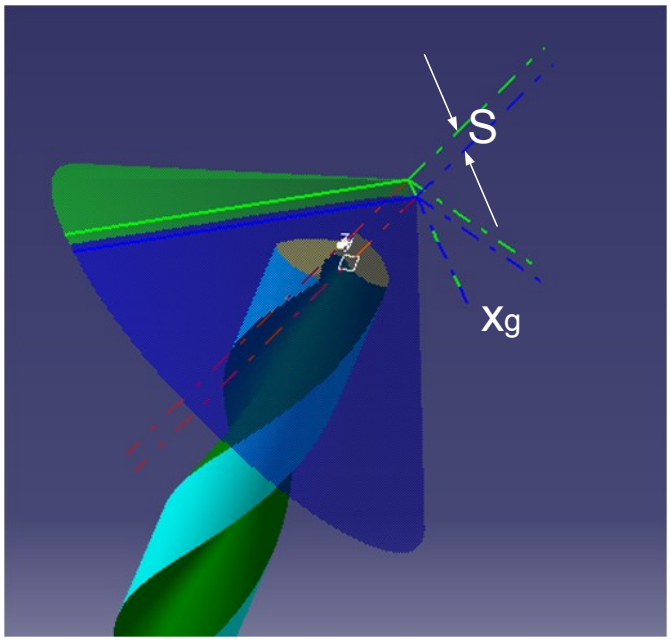

Figure 4-5 Conical flank modeling: Step 4

Fifth, the cone and its coordinate system translates along its y-axis with d_y.

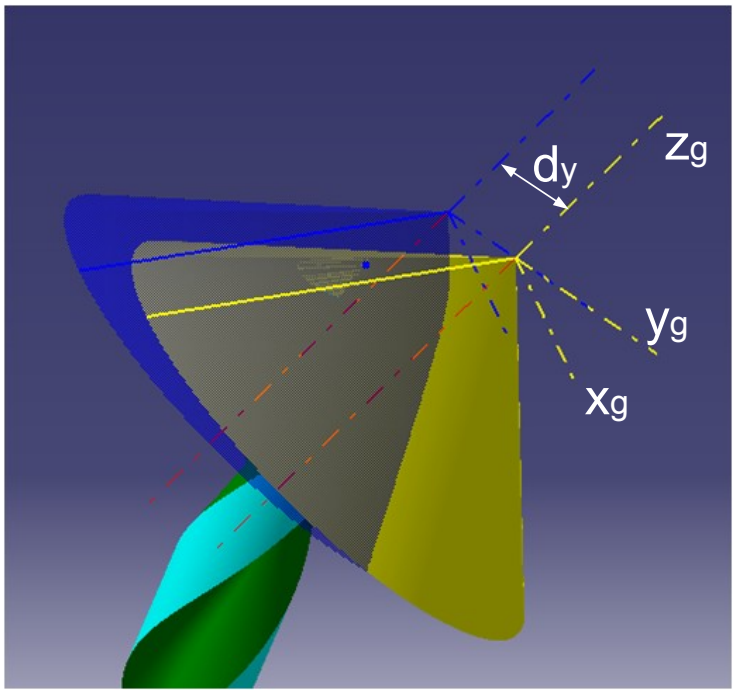

Figure 4-6 Conical flank modeling: Step 5

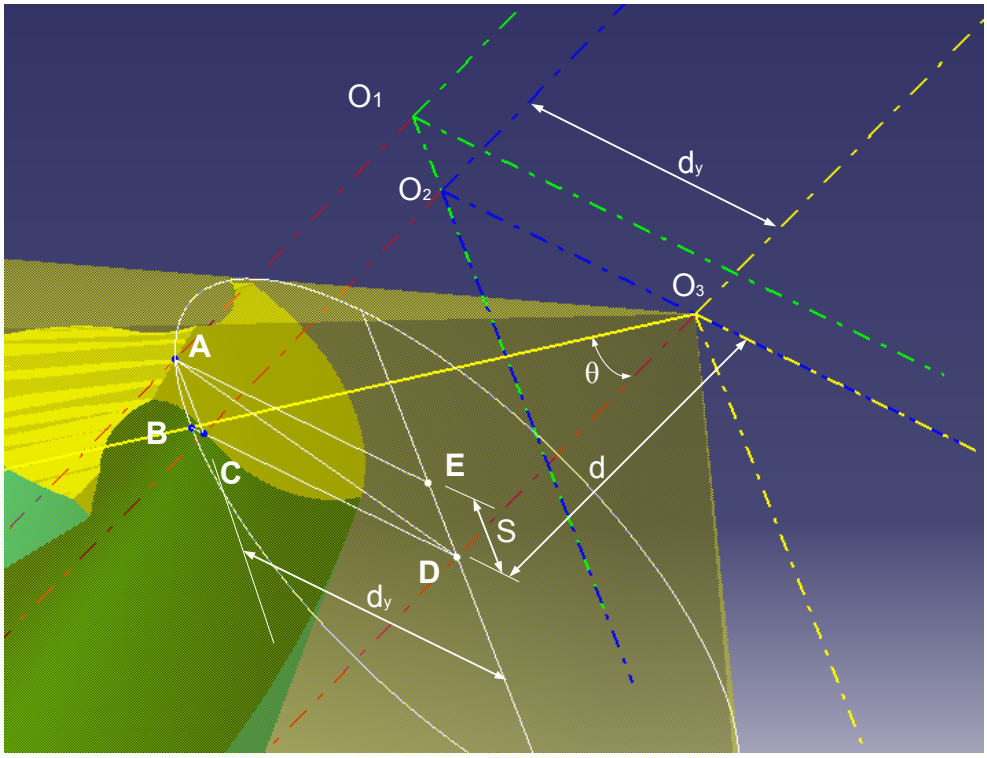

Figure 4-7 Calculation of d_y

It is important to define the tip of the drill point as the origin of the drill system. However, the tip is formed by the two cone surfaces after grinding the two flanks. So, the cone surfaces should pass through the origin, say, point A, of the drill system. To ensure this requirement, the translation d_y is calculated as below.

$\overline{AD}$ and $\overline{BD}$ are the radius of the white circle.

$$\overline{AD} = \overline{BD} = d \cdot \tan\theta$$

$\overline{DE}$ is the stew distance *S*.

$$\overline{DE} = S$$

Thus,

$$d_y \equiv \overline{CD} = \overline{AE} = \sqrt{\left(\overline{AD}\right)^2 - \left(\overline{DE}\right)^2} = \sqrt{\left(d \cdot \tan\theta\right)^2 - S^2} \tag{4.5}$$

Substituting the values of d, θ and S,

$$d_y = \sqrt{\left(10 \cdot \tan 45°\right)^2 - 3^2} = 9.539mm$$

.

Finally, to get better distribution of relief angles along the cutting lip, the cone surface and it coordinate system rotate about z_d with angle ω.as shown in Figure 4-8. The red, green, and blue squares represent $x_g z_g$, $x_g y_g$, and $y_g z_g$ planes, respectively.

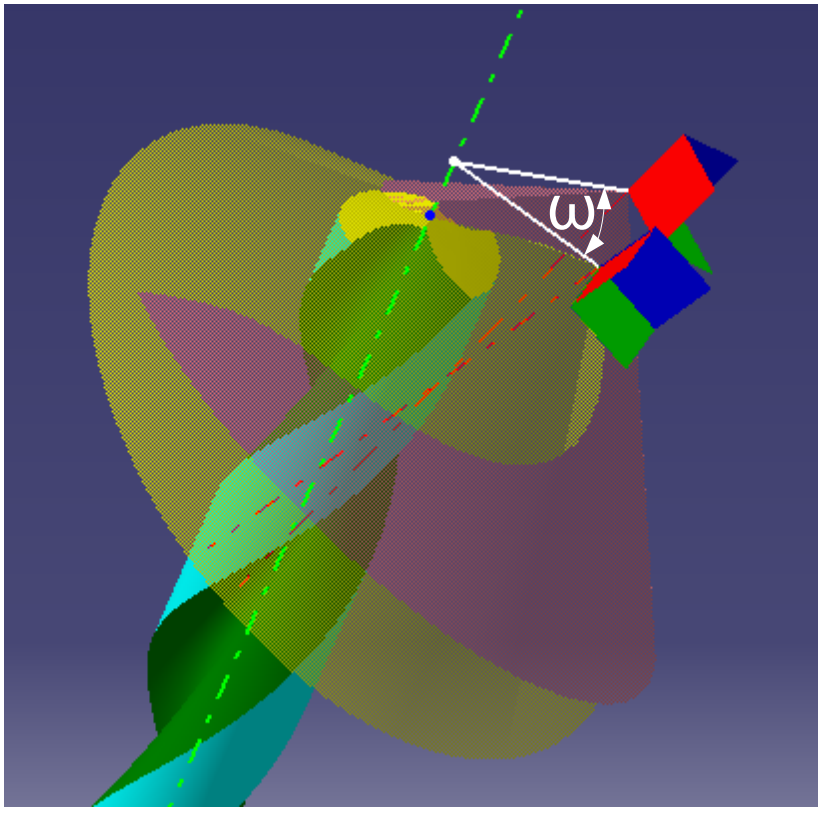

Figure 4-8 Conical flank modeling: Step 6

According to the above process modeling, the transformation matrix from the drill coordinate system to the final cone coordinate system is

$$
\begin{aligned}
{}^{g}_{d}\mathbf{M} &= \mathbf{M}^{T}(-S,0,0)\cdot\mathbf{M}^{T}(0,-d_{y},0)\cdot\mathbf{M}^{T}(0,0,-d)\cdot\mathbf{M}^{R}(x_{g},\phi)\cdot\mathbf{M}^{R}(z_{g},-\omega) \\
&= \begin{bmatrix} \cos\omega & \sin\omega & 0 & -S \\ -\cos\phi\cdot\sin\omega & \cos\phi\cdot\cos\omega & -\sin\phi & -\sqrt{(d\cdot\tan\theta)^{2}-S^{2}} \\ -\sin\phi\cdot\sin\omega & \sin\phi\cdot\cos\omega & \cos\phi & -d \\ 0 & 0 & 0 & 1 \end{bmatrix}
\end{aligned} \tag{4.5}
$$

$$
\begin{aligned}
\mathbf{S}_{g} &= {}^{g}_{d}\mathbf{M}*\mathbf{S}_{d} \\
\begin{bmatrix} x_{g} \\ y_{g} \\ z_{g} \\ 1 \end{bmatrix} &= \begin{bmatrix} \cos\omega & \sin\omega & 0 & -S \\ -\cos\phi\sin\omega & \cos\phi\cos\omega & -\sin\phi & -\sqrt{(d\tan\theta)^{2}-S^{2}} \\ -\sin\phi\sin\omega & \sin\phi\cos\omega & \cos\phi & -d \\ 0 & 0 & 0 & 1 \end{bmatrix}\begin{bmatrix} x_{d} \\ y_{d} \\ z_{d} \\ 1 \end{bmatrix} \\
&= \begin{bmatrix} (x_{d}\cos\omega + y_{d}\sin\omega) - S \\ (-x_{d}\sin\omega + y_{d}\cos\omega)\cos\phi - z_{d}\sin\phi - \sqrt{(d\tan\theta)^{2}-S^{2}} \\ (-x_{d}\sin\omega + y_{d}\cos\omega)\sin\varphi + z_{d}\cos\varphi - d \\ 1 \end{bmatrix}
\end{aligned} \tag{4.6}
$$

Calling Equation (4.2), the mathematical model for the conical flank is

$$
\begin{aligned}
&\left((x_{d}\cos\omega + y_{d}\sin\omega) - S\right)^{2} \\
&+\left((-x_{d}\sin\omega + y_{d}\cos\omega)\cos\phi - z_{d}\sin\phi - \sqrt{(d\tan\theta)^{2}-S^{2}}\right)^{2} \\
&-\tan^{2}\theta\left((-x_{d}\sin\omega + y_{d}\cos\omega)\sin\varphi + z_{d}\cos\varphi - d\right)^{2} = 0
\end{aligned} \tag{4.7}
$$

4.3 Parametric modeling of the planar flanks

To build a parametric model of the planar flanks of the twist drill tip, the relief and the point angles are taken as the parameters. After the grinding wheel is properly oriented,

a flat flank can be grinded with the side of the wheel in a path. Since the manufacturing process is quite simple, its model can be easily established.

The main steps of constructing a planar flank of the drill tip include four steps, which are described in the following.

Assuming the cutter coordinate system initially is set up at the center of the bottom plane of the cutter and its Z axis is aligned with the cutter axis and points towards the tool shank. First step, this coordinate system is translated along its positive X axis direction by a half of the web thickness. This coordinate system at the two locations is plotted in the following diagram.

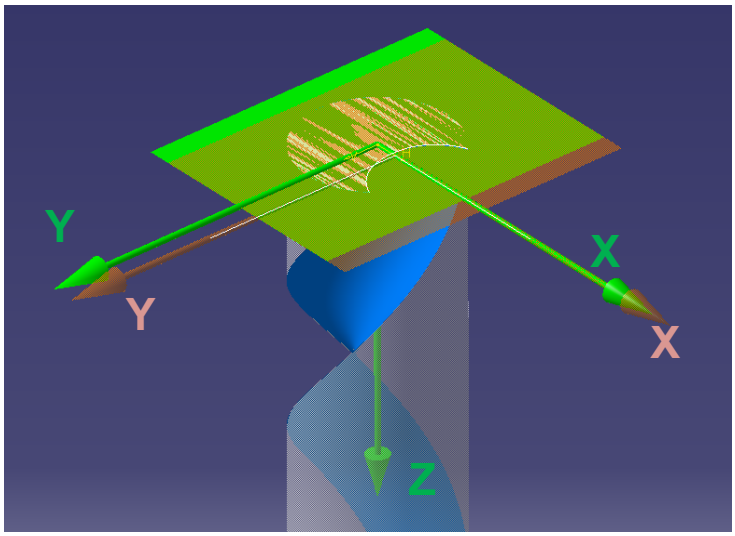

Figure 4-9 The cutter coordinate system is translated along its positive X axis direction by a half of the web thickness.

Second, rotate the cutter coordinate system about its X axis by a half of the drill point angle, shown in the following diagram.

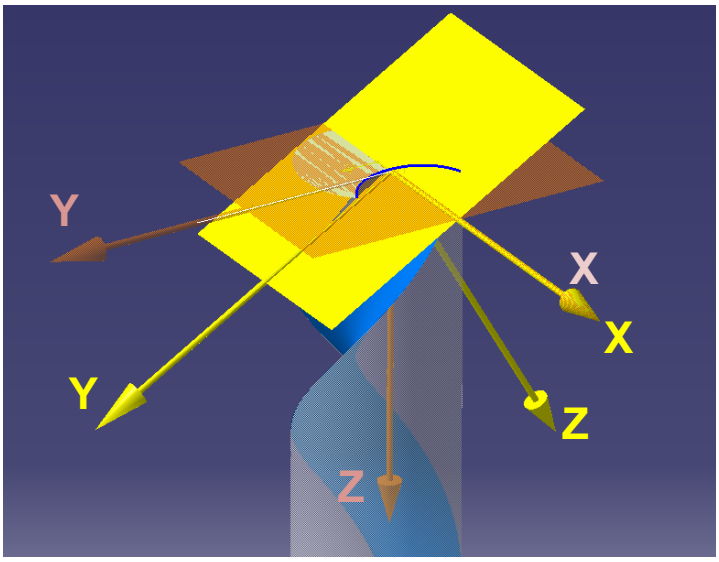

Figure 4-10 The cutter coordinate system is rotated around its X axis by a half of the drill point angle.

Third, the cutter coordinate system is rotated around its Y axis by the relief angle.

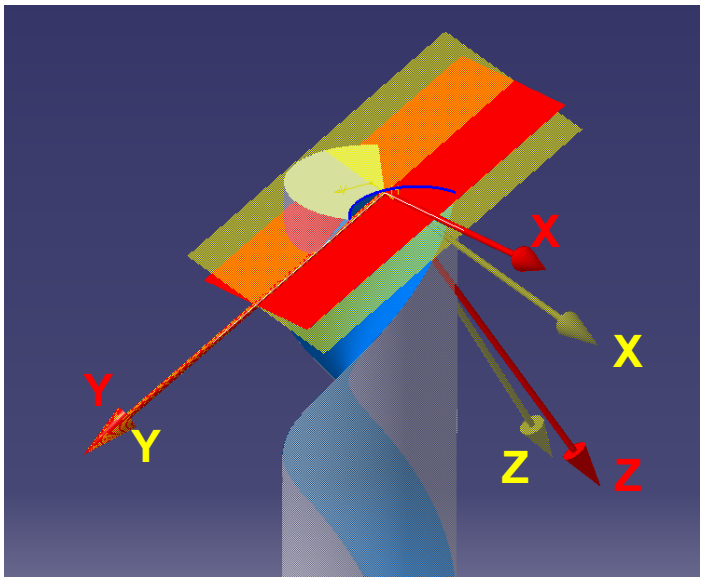

Figure 4-11 The cutter coordinate system is rotated about its Y axis by the relief angle.

The plane passing through the X and the Y axes represent the flank face of the twist drill tip. The plane is shown in red in the following diagram, and, by applying the Boolean

operation - removing, a flank face is finally generated in the solid model of the drill.

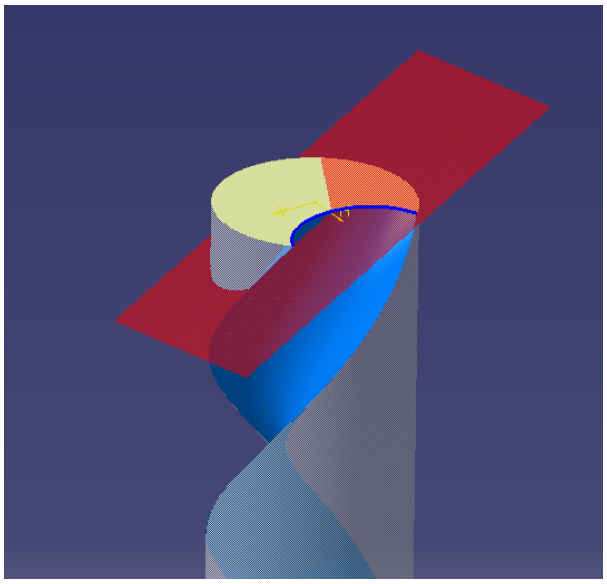

Figure 4-12 The final grinding wheel position

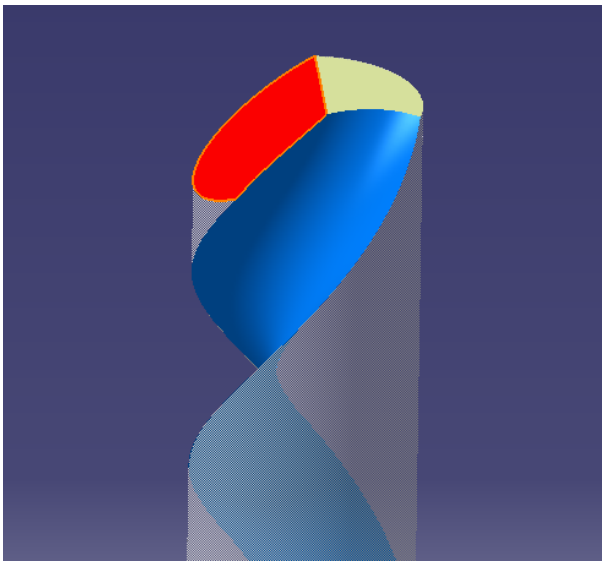

Figure 4-13 The solid model of a twist drill with a flank face generated.

Chapter 5 Drill Split Modeling

5.1 Introduction

The twist drill performance is often measured with the thrust force and the torque during machining. Among the features that affect the drill performance, the chisel edge is particular significant. Since the rake angle of the chisel edge is negative, during drilling, the chisel edge locates the drill at a position on the part surface and generates a large amount of thrust force. Therefore, the length of the chisel edge should be optimized for a drill with a long chisel edge generates a large thrust force and a drill without the chisel edge cannot be located while machining. To address this problem, the drill split (also called the drill gash) is widely adopted in the drill manufacturing industry. The main advantage of drill split is that the chisel edge is shortened and a secondary cutting edge is generated with positive rake angles. Thus, the drill split can effectively solve the problems of conventional twist drills. In this thesis, the parametric model of the drill split is established; the detailed procedure will be introduced in the following section; and, based on the machining features, a mathematical model of the drill split is firstly proposed. By optimizing the drill split parameters, the best drill performance can be achieved.

5.2 Parametric Modeling of the Drill Split

The parametric model of the drill split includes some parameters, such as the gash angle to XY plane, the gash axis, the location of the starting point, the rake angles at the starting and the ending points of the gash (axial rake at tip and axial rake at center), and the exit angle (walk angle) etc. these parameters defines the gash features. For example, the gash axis is determined by the 'S gash offset', 'S gash radius', and 'Gash angle in XY plane'. Based on the drill split parameters, the drill split can be modeled with CATIA V5.

Table 5-1 Parameters for drill split modeling

Parameters	Value used in this model 1
Basic gash angle	55°
Gash angle in XY plane	-8°
Axial rake at tip	5°
Axial rake at center	0°
S gash radius	1.5 mm
S gash offset	0.1 mm
Walk angle	100°
Walk length	12 mm
Gashing wheel diameter	120 mm

5.2.1 Construction of the Drill Split

At the starting point of the drill gash, draw a helix guide with the helix angle equal to the gash angle and around the gash axis. The helix stops at the ending point of the gash. The helix guide is shown in white in the following diagram.

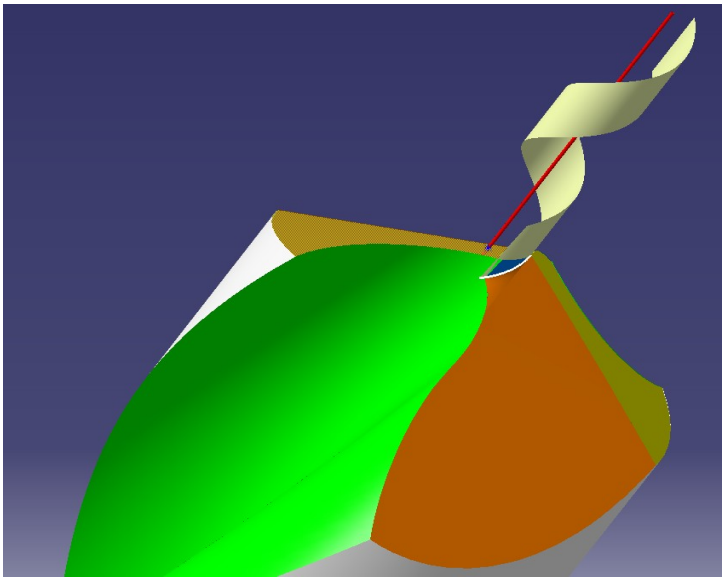

Figure 5-1 The helix guide is drawn in order to machine the gash.

According to the rake angle at the starting point of the gash, draw the grinding wheel. Based on the rake angle at the ending point of the gash, the rake face can be generated by sweeping the effective grinding edge along the helix guide. The rake face is shown in the following diagram in blue.

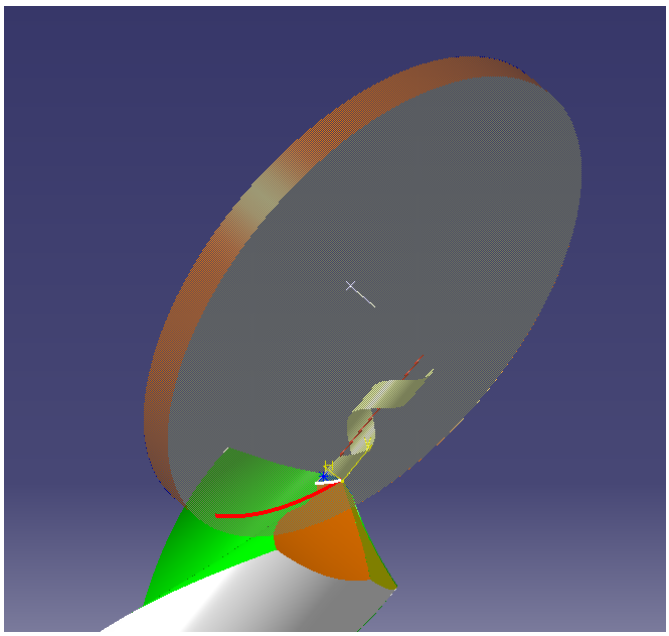

Figure 5-2 The grinding wheel is located at the starting point of the drill split.

According to the exit angle of the gash, a guide curve is defined shown in the following diagram. Based on the guide, the effective grinding edge of the wheel is found, and the surface is swept along the guide curve is generated. Using the Split operation, remove, the gash and the second flank face are generated, which are shown in the following diagram.

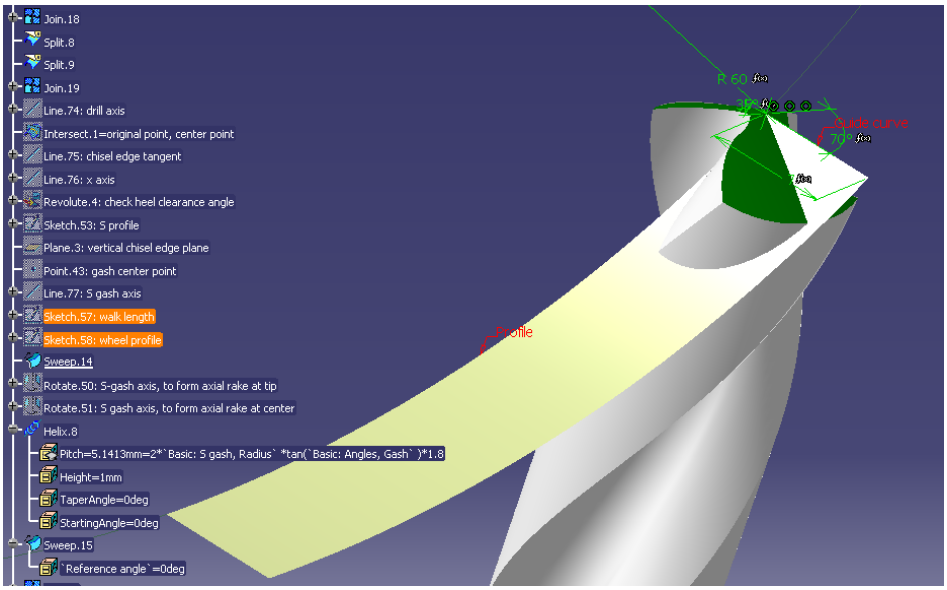

Figure 5-3 The second flank is generated by removing the drill stock with the surface swept by the effective grinding edge along the guide curve.

The drill split (or gash) and its second flank are generated, and a drill with a gash is shown in the following diagram.

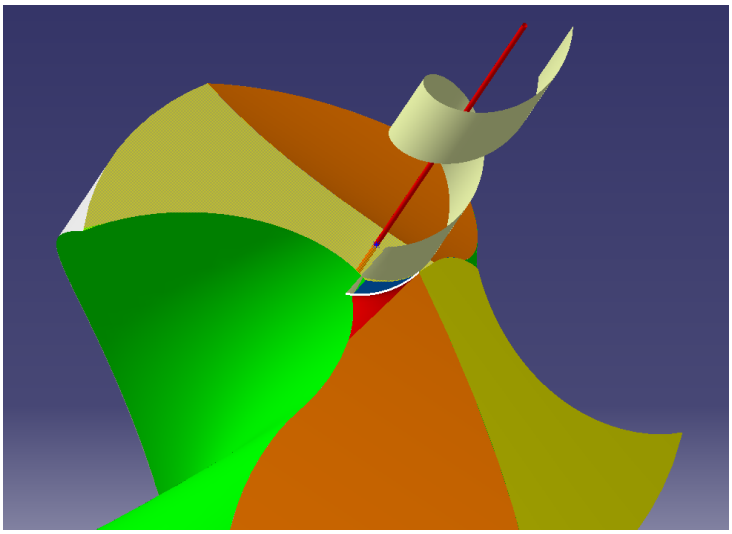

Figure 5-4 A drill with a blue gash and the orange second flank are shown

5.2.2 Mathematical model of the gash

Assuming the gashing axis is a unit vector $\vec{\mathbf{K}} = [k_1 \quad k_2 \quad k_3]^T$ at the position $\mathbf{P} = [p_1 \quad p_2 \quad p_3]^T$, the transformation matrix for helically rotating around the axis of the helical guide line is

$$\mathbf{R}_{\vec{K}} = Trans([p_1 \quad p_2 \quad p_3]) \cdot Rot(\vec{K}, \theta) \cdot Trans(\lambda\theta\vec{K}) \cdot Trans([-p_1 \quad -p_2 \quad -p_3])$$

$$= \begin{bmatrix} k_1^2(1-\cos\theta)+\cos\theta & k_1k_2(1-\cos\theta)-k_3\cdot\sin\theta & k_1k_3(1-\cos\theta)+k_2\cdot\sin\theta & p_1 \\ k_1k_2(1-\cos\theta)+k_3\cdot\sin\theta & k_2^2(1-\cos\theta)+\cos\theta & k_2k_3(1-\cos\theta)-k_1\cdot\sin\theta & p_2 \\ k_1k_3(1-\cos\theta)-k_2\cdot\sin\theta & k_2k_3(1-\cos\theta)+k_1\cdot\sin\theta & k_3^2(1-\cos\theta)+\cos\theta & p_3 \\ 0 & 0 & 0 & 1 \end{bmatrix} \begin{bmatrix} 1 & 0 & 0 & \lambda\cdot k_1\cdot\theta - p_1 \\ 0 & 1 & 0 & \lambda\cdot k_2\cdot\theta - p_2 \\ 0 & 0 & 1 & \lambda\cdot k_3\cdot\theta - p_3 \\ 0 & 0 & 0 & 1 \end{bmatrix}$$

Let

$$Trans([p_1 \quad p_2 \quad p_3]) \cdot Rot(\vec{K}, \theta) = \begin{bmatrix} a_{11} & a_{12} & a_{13} & p_1 \\ a_{21} & a_{22} & a_{23} & p_2 \\ a_{31} & a_{32} & a_{33} & p_3 \\ 0 & 0 & 0 & 1 \end{bmatrix}$$

then

$$\mathbf{R}_{\vec{K}} = \begin{bmatrix} a_{11} & a_{12} & a_{13} & p_1 \\ a_{21} & a_{22} & a_{23} & p_2 \\ a_{31} & a_{32} & a_{33} & p_3 \\ 0 & 0 & 0 & 1 \end{bmatrix} \begin{bmatrix} 1 & 0 & 0 & \lambda\cdot k_1\cdot\theta - p_1 \\ 0 & 1 & 0 & \lambda\cdot k_2\cdot\theta - p_2 \\ 0 & 0 & 1 & \lambda\cdot k_3\cdot\theta - p_3 \\ 0 & 0 & 0 & 1 \end{bmatrix}$$

$$= \begin{bmatrix} a_{11} & a_{12} & a_{13} & a_{11}(\lambda\cdot k_1\cdot\theta - p_1) + a_{12}(\lambda\cdot k_2\cdot\theta - p_2) + a_{13}(\lambda\cdot k_3\cdot\theta - p_3) + p_1 \\ a_{21} & a_{22} & a_{23} & a_{21}(\lambda\cdot k_1\cdot\theta - p_1) + a_{22}(\lambda\cdot k_2\cdot\theta - p_2) + a_{23}(\lambda\cdot k_3\cdot\theta - p_3) + p_2 \\ a_{31} & a_{32} & a_{33} & a_{31}(\lambda\cdot k_1\cdot\theta - p_1) + a_{32}(\lambda\cdot k_2\cdot\theta - p_2) + a_{33}(\lambda\cdot k_3\cdot\theta - p_3) + p_3 \\ 0 & 0 & 0 & 1 \end{bmatrix} \quad (5.1)$$

The formula (5.1) is the general transformation matrix for gashing process.

Assuming the axis of the helical guide line (denoted by Z_{gash}) is parallel to the end surface of the grinding wheel (denoted by S_{end}), the rake surface of the gash then can be simplified as a swept surface created by a straight-line profile, which is parallel to the Z_{gash} and on the S_{end}, sweeping along a helical guide curve.

The straight-line profile is:

$$\begin{aligned}\mathbf{L}_{staight} &= \vec{\mathbf{q}} + m\vec{\mathbf{k}} \\ &= \begin{bmatrix} q_1 + m\cdot k_1 & q_2 + m\cdot k_2 & q_3 + m\cdot k_3 \end{bmatrix}\end{aligned}$$

The swept surface or the rake face, $\mathbf{S}_{r,g}$, of the gashing is:

$$\begin{aligned}\mathbf{S}_{r,g} &= \mathbf{R}_{\vec{k}} \ldots_{aight} \\ &= \begin{bmatrix} a_{11} & a_{12} & a_{13} & a_{11}(\lambda\cdot k_1\cdot\theta - p_1) + a_{12}(\lambda\cdot k_2\cdot\theta - p_2) + a_{13}(\lambda\cdot k_3\cdot\theta - p_3) + p_1 \\ a_{21} & a_{22} & a_{23} & a_{21}(\lambda\cdot k_1\cdot\theta - p_1) + a_{22}(\lambda\cdot k_2\cdot\theta - p_2) + a_{23}(\lambda\cdot k_3\cdot\theta - p_3) + p_2 \\ a_{31} & a_{32} & a_{33} & a_{31}(\lambda\cdot k_1\cdot\theta - p_1) + a_{32}(\lambda\cdot k_2\cdot\theta - p_2) + a_{33}(\lambda\cdot k_3\cdot\theta - p_3) + p_3 \\ 0 & 0 & 0 & 1 \end{bmatrix} \begin{bmatrix} q_1 + m\cdot k_1 \\ q_2 + m\cdot k_2 \\ q_3 + m\cdot k_3 \\ 1 \end{bmatrix}\end{aligned}$$

(5.2)

It is a surface with two variables

$$\mathbf{S}_{r,g} = \mathbf{S}_{r,g}(\theta,\ m)$$

For example, if

$$\vec{\mathbf{k}} - \begin{bmatrix} \upsilon & 0 & 1 \end{bmatrix}^T$$

$$\mathbf{P} = \begin{bmatrix} p_1 & p_2 & 0 \end{bmatrix}^T,$$

then

$$\begin{aligned}\mathbf{R}_{\vec{k}} &= Trans\left(\begin{bmatrix} p_1 & p_2 & p_3 \end{bmatrix}\right) Rot\left(\vec{\mathbf{k}},\ \upsilon\right) Trans\left(\lambda\upsilon\vec{\mathbf{k}}\right) Trans\left(\begin{bmatrix} -p_1 & -p_2 & -p_3 \end{bmatrix}\right) \\ &= \begin{bmatrix} \cos\theta & -\sin\theta & 0 & p_1 \\ \sin\theta & \cos\theta & 0 & p_2 \\ 0 & 0 & 1 & 0 \\ 0 & 0 & 0 & 1 \end{bmatrix} \begin{bmatrix} 1 & 0 & 0 & -p_1 \\ 0 & 1 & 0 & -p_2 \\ 0 & 0 & 1 & \lambda\theta \\ 0 & 0 & 0 & 1 \end{bmatrix} \\ &= \begin{bmatrix} \cos\theta & -\sin\theta & 0 & p_1(1-\cos\theta) + p_2\cdot\sin\theta \\ \sin\theta & \cos\theta & 0 & p_2(1-\cos\theta) - p_1\cdot\sin\theta \\ 0 & 0 & 1 & \lambda\theta \\ 0 & 0 & 0 & 1 \end{bmatrix},\end{aligned}$$

$$\mathbf{L}_{staight} = \vec{\mathbf{q}} + m\vec{\mathbf{k}}$$
$$= \begin{bmatrix} q_1 & q_2 & q_3 + m \end{bmatrix},$$

and,

$$\mathbf{S}_{r,g} = \mathbf{R}_{\vec{k}\ \ldots aight}$$
$$= \begin{bmatrix} \cos\theta & -\sin\theta & 0 & p_1(1-\cos\theta) + p_2 \cdot \sin\theta \\ \sin\theta & \cos\theta & 0 & p_2(1-\cos\theta) - p_1 \cdot \sin\theta \\ 0 & 0 & 1 & \lambda \cdot \theta \\ 0 & 0 & 0 & 1 \end{bmatrix} \begin{bmatrix} q_1 \\ q_2 \\ q_3 + m \\ 1 \end{bmatrix}.$$

Thus,

$$\mathbf{S}_{r,g} = \mathbf{R}_{\vec{k}\ \ldots aight}$$
$$= \begin{bmatrix} q_1 \cdot \cos\theta - q_2 \cdot \sin\theta + p_1(1-\cos\theta) + p_2 \cdot \sin\theta \\ q_1 \cdot \sin\theta + q_2 \cdot \cos\theta + p_2(1-\cos\theta) - p_1 \cdot \sin\theta \\ q_3 + m + \lambda \cdot \theta \\ 1 \end{bmatrix} = \begin{bmatrix} x_{r,g}(\theta) \\ y_{r,g}(\theta) \\ z_{r,g}(m, \quad \theta) \\ 1 \end{bmatrix} \tag{5.3}$$

It can be seen that

$$\left(x_{r,g}(\theta) - p_1\right)^2 + \left(y_{r,g}(\theta) - p_2\right)^2 = \left(q_1 - p_1\right)^2 + \left(q_2 - p_2\right)^2 = const1 \tag{5.4}$$

The above equation shows that the $S_{r,g}$ is a part of a cylinder surface with the radius equal to $\sqrt{\left(q_1 - p_1\right)^2 + \left(q_2 - p_2\right)^2}$.

5.3 Final model of manufacturing feature-based twist drill

In this thesis, the other features of twist drill like the lands, the internal cooling holes, and etc., are relatively simple; and they are not shown in details although they were completed in final model.

Figure 5-5 shows the drill point with gashing done.

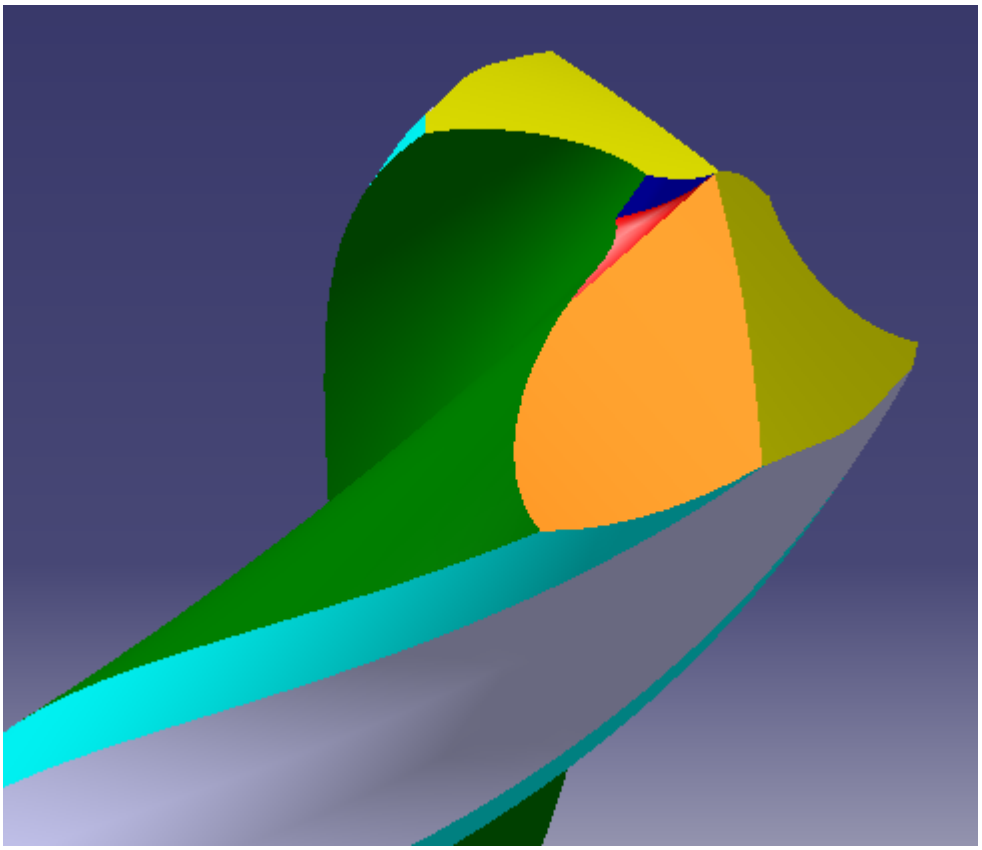

Figure 5-5 Drill point with gashing done

Figure 5-6 shows the final parametric model for machining feature-based twist drill. The geometric features, such as the body, the flutes, the flanks, the radius splits, the internal cooling holes, and the land, are well completed. This model exactly reflects the grinding features if the grinding errors, such as vibration errors, are ignore.

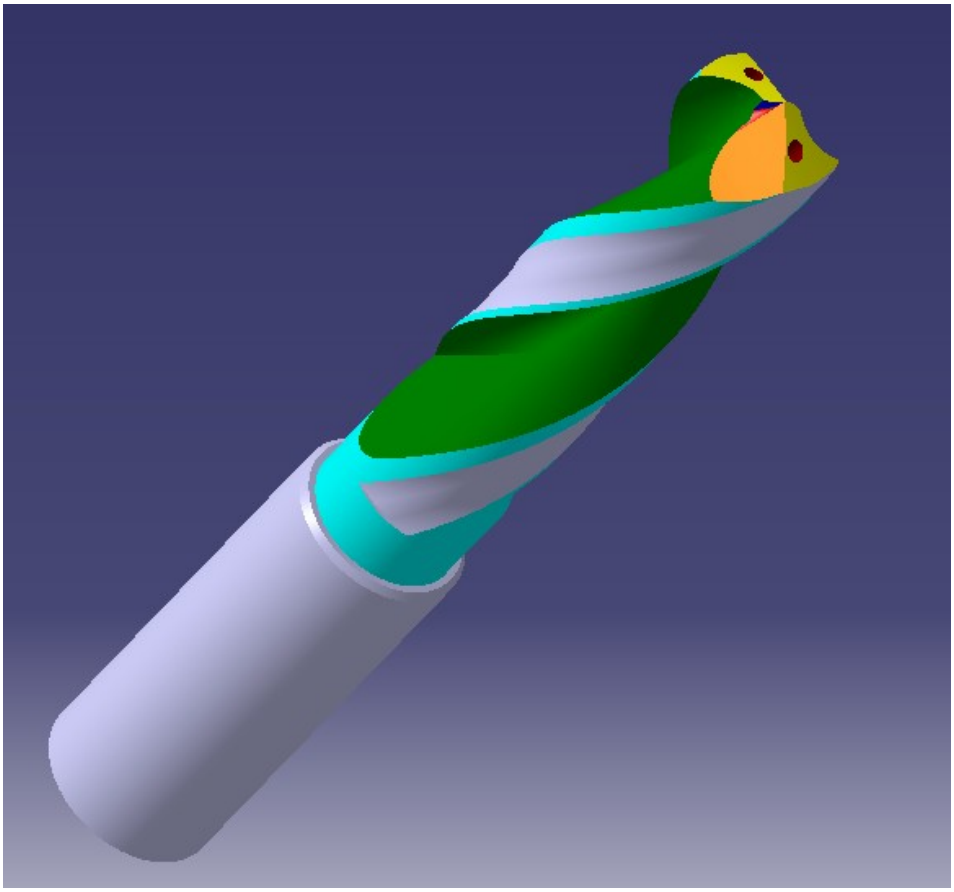

Figure 5-6 Final machining feature-based geometric model of twist drill

Chapter 6 Conclusion & Future Work

6.1 Conclusion

The thesis of developing a manufacturing feature-based solid twist drill is now completed. The main objective is the build the accurate parametric solid models of the solid twist drill based on their manufacturing and geometric features. The main geometric features of the drills are provided in the following.

The flutes. The mathematical model of the flute, the direct method and inverse method to design and build the flutes, and the steps to build the geometric model are provided. The problem to connect the flute with the land have been solved in this thesis.

The flanks. The mathematical models for quadratic and planar flanks are provided. Steps to build the parametric solid models for a conical flank and a planar flank are described.

The drill split. The steps to build the gash features are provided. A new mathematical model for the radius split is first proposed in this thesis.

The parametric models of these features have been established, and they have been implemented with the CATIA V5 R20 to build the solid models of a twist drill. These models are genuine models of the actually machined cutters. Therefore, using these models is essential to predict machining performance of the actual cutters with the finite element analysis.

6.2 Future Work

The future work of modeling the twist drill will focus on calibrating the solid models of the twist drill based on their actual manufacturing processes and conducting finite element analysis on the tools to simulate their machining performance. Based on the result, a number of drills will be made and extensive cutting tests will be carried out. Meanwhile, the dynamic models of the tools will be established in order to predict the tool vibration during machining.

References

(1) JT. Black, and Ronald A. Kohser, 2008, “DeGarmo's Material & Process in Manufacturing”, *John Wiley & Sons, Inc.,* pp. 628-629.

(2) S. Engin, and Y. Altintas, 2001, “Mechanics and dynamics of general milling cutters. Part I: helical end mills,” *International Journal of Machine Tool & manufacture*, Vol. 41, pp. 2195-2212.

(3) D.F. Galloway, “Some Experiments on the Influence of Various Factors on Drill Performance”, Transactions of the ASME, 1957, pp. 191–231.

(4) E.J.A. Armarego and A. Rotenberg, “An investigation of drill point sharpening by the straight lip conical grinding method—II. A criterion for selecting a solution”, *Int. J. Mach. Tool Des*., 1973, 13(4), pp. 165-182.

(5) E.J.A. Armarego and A. Rotenberg, “An investigation of drill point sharpening by the straight lip conical grinding method—III. Drill point grinder design features”, *Int. J. Mach. Tool Des*., 1973, 13(4), pp. 233-241.

(6) W. Tsai, and S.M. Wu, “A mathematical model for drill point design and grinding”, *Journal of Engineering for Industry*, 1979, pp. 333–340.

(7) T. Radhakrishnan, S.M. Wu and C. Lin, “A mathematical model for split point drill flanks”, ASME *Journal of Engineering for Industry*, 1983, pp. 137–142.

(8) M.A. Fugelso, “Conical flank twist drill points", *International Journal of Machine Tools and Manufacture*, 1990, 30(2), pp. 291-295.

(9) C. Lin, S.K. Kang, K.F. Ehmann, "Helical Micro-drill Point Design and Grinding", *Journal of Engineering for Industry,* 1995, 117(3): 277-287

(10) K.C. Ren, “Analyses of drill flute and cutting angles”, *International Journal of Advanced Manufacturing Technology*, 1999, 15(8), pp. 546-553.

(11) Wang, Ger-Chwang, Fuh et., “Mathematical Model for Multifacet Drills Derived by using Angle-solid model”, *International Journal of Machine Tools and Manufacture*, 2001, 41(1), pp. 103-132.

(12) S. Kaldor, A.D. Rafael and D. Messinger, “On the CAD of Profiles for Cutters and Helical Flutes - Geometrical Aspects,” *Annals of CIRP*, 1988, pp. 53–56

(13) K.F. Ehmann, M.F. DeVries, “Grinding Wheel Profile Definition for the Manufacture of Drill Flutes”, CIRP Annals - *Manufacturing Technology*, 1990, 39(1), pp. 153-156.

(14) J.F. Hsieh, “Mathematical model for helical drill point,” International Journal of Machine Tools & Manufacture, 2005, 45(7-8), pp. 967-977

(15) S. Fujii, M.F. DeVries, and S.M. Wu, “An analysis of drill geometry for optimum drill design by computer Part I- Drill geometry analysis”, *Journal of Engineering for Industry*, 1970, 92(3), pp. 647–656.

(16) S. Fuji, M.F. DeVries, and S.M. Wu, “An analysis of drill geometry for optimum drill design by computer. part II - computer aided design”, *Journal of Engineering for Industry*, 1970, 92(3), pp. 657–666.

(17) K.H. Fuh, G.C. Wang, C.C. Tai, “Computer aided design for drill geometry by quadratic surface model”, *Conf. on Production Research*, 1985, pp.425-430

(18) Sheth, D.S., and Malkin, S., 1973, “CAD/CAM for geometry and process analysis of helical flute machining,” *Annals of CIRP*, Vol. 22, No. 1, pp. 157-164.

(19) Kaldor, S., Rafael, A.M., and Messinger, D., 1990, “On the CAD of profiles for cutters and helical flutes – geometrical aspects,” *Annals of CIRP*, Vol. 39, No. 1, pp. 129-132.

(20) Kang, S.K., Ehmann, K.F., and Lin, C., 1996, “A CAD approach to helical flute machining, I. mathematical model and model solution,” *International Journal of Machine Tools & Manufacturing,* Vol. 36, No. 1, pp. 141-153.

(21) A. Vijayaraghavan and D.A. Dornfeld, “Automated drill modeling for drilling process simulation,” Journal of Computing and Information Science in Engineering, 2007, 7(3), pp. 276–282.

(22) M.Y. Li, T. Shen, D.Q. Wang, "The Simulation Measurement of Standard Twist Drill's Angle Based on PRO/E", *Modular Machine Tool & Automatic Manufacturing techniques*, 2010, n3, 68-70

Appendix A

Code for Direct Method to find EGE by a standard parallel wheel

```
clear all
close all

syms  c L a v real
syms az ax ax0 k1 k3 xh xph zh zph column4 h real

%a = alpha;  = 'rake angle' about y axis
%L = lambda = related to helix angle
%k1 = parameter related to conical surface
%k3 = lead
%ax0 = initial distance between wheel axis and drill axis
%R = drill radius
%xh zh = related to generating curve
%c = helical rotating angle about drill axis
%v = revolution angle of generating curve about wheel axis
%h = parameter of generating curve

 % basic information------------------------------

R_wheel = 75;
R1 = .05;
R2 = .05;
W = 18;
W_angle = double(90/180*pi); % this angle is between 15 and 90 degree; parallel wheel
has an angle of 90 degree
R = 6;
R_core = R*1/4;
a = 25*pi/180;
L = 60*pi/180;
k1 = 0.00318;
k3 = tan(L)*R;

Rwl_Rcn_W = [R_wheel,R1,R2,W,W_angle,R];
%-------------------------------------------------

qt = [xh,0,zh,1]';  %qt = generating curve
rt = Rz(v)*qt;      %rt = wheel surface
```

```
rh = [xph*cos(v),xph*sin(v),zph]; %rh=d(rt)/d(h)
rt_33 = rt(1:3);
rv = diff(rt_33,v);             %rv=d(rt)/d(v)

A0t = Rx(pi)*T([0 0 az])*Rz(c)*Rx(L)*Ry(a)*T([ax 0 0]);

ax0 = R_wheel+R_core/cos(a);
ax = ax0+k1*c;
az = k3*c;

A0t1 = subs(subs(A0t,'ax',ax),'az',az);
T11 = diff(A0t1,c);
A0t_33 = A0t1(1:3,1:3);

Colum1 = T11*rt; % = partial differentiation to thelda or time
Colum2 = A0t_33*rh';
Colum3 = A0t_33*rv;
Bcross = simplify(cross(Colum2,Colum3));
Colum1_3 = Colum1(1:3);
ConjResult = dot(Colum1_3,Bcross);

Conj03 = simplify(ConjResult/xh);  %Conj03 should =0

%-----------------------------------------------------

n = 82;
pi = double(pi);


H1 = R_wheel-R1;
H0 = H1-R*1.5;
H2 = H1+R1*(double(pi)-W_angle);
H3 = H2+W/sin(W_angle)-R1/tan(W_angle/2)-R2*tan(W_angle/2);
H4 = H3+R2*W_angle;
H5 = H4+R*1.5;


H_flag(1) = double((H0+H1)/2);
H_flag(2) = double((H1+H2)/2);
H_flag(3) = double((H2+H3)/2);
H_flag(4) = double((H3+H4)/2);
H_flag(5) = double((H4+H5)/2);
Coneq = [];
```

```
crosscurvex = [];
crosscurvey = [];
crosscurvez = [];
digits 12
for i=1:5

    [xh,zh,xph,zph]=xh_zh_xph_zph_angle(h,Rwl_Rcn_W,H_flag(i));
    rt1 = subs(rt);
    [Con2,crscurvex,crscurvey,crscurvez]= Conjeqation02(rt1,Conj03,A0t1);
    Coneq = [Coneq;Con2];
    crosscurvex = vpa([crosscurvex;crscurvex]);
    crosscurvey = vpa([crosscurvey;crscurvey]);
    crosscurvez = vpa([crosscurvez;crscurvez]);

end

H_step0 = (H1-H0)/n;
H_stepI = (H2-H1)/n;
H_stepII = 2*(H3-H2)/n;
H_stepIII = (H4-H3)/n;

for i=1:n+1
    H_end(i,1) = H0 + H_step0*(i-1);
end

for i=1:n+1
    H_corner(i,1) = H1+H_stepI*(i-1);
    H_corner(i,2) = H3+H_stepIII*(i-1);
end

n_center = floor(n/2);

for i=1:n_center+1
    H_center(i,1) = H2+H_stepII*(i-1);
end

H = [H_end(:,1);H_corner(:,1);H_center(:,1);H_corner(:,2)];

vvalue = [];
cvalue = [];

prepointv = double(pi*7/8);
hvalue = [];
crsxvalue1 = [];
```

```
crsyvalue1 = [];
crszvalue1 = [];

crsxvalue2 = [];
crsyvalue2 = [];
crszvalue2 = [];

crsxvalue3 = [];
crsyvalue3 = [];
crszvalue3 = [];

crsxvalue4 = [];
crsyvalue4 = [];
crszvalue4 = [];

digits 15;

n0 = n + 1;
n1 = n0 + n + 1;
n2 = n1 + n_center + 1;
n3 = n2 + n + 1;
for j=1:n3
    if j<=n0
        eq1=vpa(subs(Coneq(1),'h',H(j)));

        [vrslt,flag] = findsolution_enhanced(eq1,prepointv);

        if flag ==1
            vvalue = [vvalue, vrslt];
            hvalue = [hvalue, H(j)];
            prepointv = vrslt;
            crsxvalue1 = [crsxvalue1,subs(subs(crosscurvex(1),'h',H(j)),'v',vrslt)];
            crsyvalue1 = [crsyvalue1,subs(subs(crosscurvey(1),'h',H(j)),'v',vrslt)];
            crszvalue1 = [crszvalue1,subs(subs(crosscurvez(1),'h',H(j)),'v',vrslt)];
        else if flag ==0
                fprintf('no solution for v and h! \n')
            end
        end
    else if j<=n1

            eq1=vpa(subs(Coneq(2),'h',H(j)));

            [vrslt,flag] = findsolution_enhanced(eq1,prepointv);
```

```
          if flag ==1
              vvalue = [vvalue, vrslt];
              hvalue = [hvalue, H(j)];
              prepointv = vrslt;
              crsxvalue2 =
[crsxvalue2,subs(subs(crosscurvex(2),'h',H(j)),'v',vrslt)];
              crsyvalue2 =
[crsyvalue2,subs(subs(crosscurvey(2),'h',H(j)),'v',vrslt)];
              crszvalue2 =
[crszvalue2,subs(subs(crosscurvez(2),'h',H(j)),'v',vrslt)];

          else if flag ==0
                 fprintf('no solution for v and h! \n')
              end
          end
       else if j<=n2
              eq1 = vpa(subs(Coneq(3),'h',H(j)));

              [vrslt,flag] = findsolution_enhanced(eq1,prepointv);

              if flag ==1
               vvalue = [vvalue, vrslt];
               hvalue = [hvalue, H(j)];
               prepointv = vrslt;
               crsxvalue3 =
[crsxvalue3,subs(subs(crosscurvex(3),'h',H(j)),'v',vrslt)];
               crsyvalue3 =
[crsyvalue3,subs(subs(crosscurvey(3),'h',H(j)),'v',vrslt)];
               crszvalue3 =
[crszvalue3,subs(subs(crosscurvez(3),'h',H(j)),'v',vrslt)];

              else if flag ==0
                  fprintf('no solution for v and h! \n')
                  end
              end
          else
             eq1 = vpa(subs(Coneq(4),'h',H(j)));

             [vrslt,flag] = findsolution_enhanced(eq1,prepointv);

             if flag ==1
                vvalue = [vvalue, vrslt];
                hvalue = [hvalue, H(j)];
                prepointv = vrslt;
```

```
                crsxvalue4 =
[crsxvalue4,subs(subs(crosscurvex(4),'h',H(j)),'v',vrslt)];
                crsyvalue4 =
[crsyvalue4,subs(subs(crosscurvey(4),'h',H(j)),'v',vrslt)];
                crszvalue4 =
[crszvalue4,subs(subs(crosscurvez(4),'h',H(j)),'v',vrslt)];

            else if flag ==0
                fprintf('no solution for v and h! \n')
                end
            end

          end
       end
   end

end

% m = length(vvalue);

digits 17;

crsxvalue1 = double(vpa(crsxvalue1));
crsyvalue1 = double(vpa(crsyvalue1));
crszvalue1 = double(vpa(crszvalue1));

crsxvalue2 = double(vpa(crsxvalue2));
crsyvalue2 = double(vpa(crsyvalue2));
crszvalue2 = double(vpa(crszvalue2));

crsxvalue3 = double(vpa(crsxvalue3));
crsyvalue3 = double(vpa(crsyvalue3));
crszvalue3 = double(vpa(crszvalue3));

crsxvalue4 = double(vpa(crsxvalue4));
crsyvalue4 = double(vpa(crsyvalue4));
crszvalue4 = double(vpa(crszvalue4));

Rcrs = [];
Rcrs(1) = crsxvalue1(1)^2+crsyvalue1(1)^2;
j = 0;
istop1 = [];

m1 = length(crsyvalue1);
```

```
for i=2:m1
    Rcrs(i) = crsxvalue1(i)^2+crsyvalue1(i)^2;
    Rtstpnt = (Rcrs(i)-R^2)*(Rcrs(i-1)-R^2);
    if Rtstpnt<0
        j=j+1;
        if j==1
            if Rcrs(i)>R*R
                istop1(1)=i;
            else
                istop1(1)=i-1;
            end
        end
        if j>=2
            if Rcrs(i)>R*R
                istop1(2)=i;
            else
                istop1(2)=i-1;
            end
            break
        end
    end

end

crsxvalue234 = [crsxvalue2,crsxvalue3,crsxvalue4];
crsyvalue234 = [crsyvalue2,crsyvalue3,crsyvalue4];
crszvalue234 = [crszvalue2,crszvalue3,crszvalue4];

Rcrs(1) = crsxvalue234(1)^2+crsyvalue234(1)^2;
m2 = length(crsyvalue234);
istop2(1) = 1;
j = 0;
for i=2:m2
    Rcrs(i) = crsxvalue234(i)^2+crsyvalue234(i)^2;
    Rtstpnt = (Rcrs(i)-R^2)*(Rcrs(i-1)-R^2);
    if Rtstpnt<0
        j=j+1;
        if j==1
            if Rcrs(i)>R*R
                istop2(1)=i;
            else
                istop2(1)=i-1;
            end
        end
```

```
        if j>=2
            if Rcrs(i)>R*R
                istop2(2)=i;
            else
                istop2(2)=i-1;
            end
            break
        end
    end

end

crsxval_fnl1 = crsxvalue1(istop1(1):istop1(2));
crsyval_fnl1 = crsyvalue1(istop1(1):istop1(2));
crszval_fnl1 = crszvalue1(istop1(1):istop1(2));
crsxval_fnl2 = crsxvalue234(istop2(1):istop2(2));
crsyval_fnl2 = crsyvalue234(istop2(1):istop2(2));
crszval_fnl2 = crszvalue234(istop2(1):istop2(2));

mm1 = length(crsxval_fnl1);
crs_xyplane1 = [];
for i = 1:mm1
    dz = -crszval_fnl1(i);
    thelta0 = double(dz/k3);
    r_z0 =
Rz(thelta0)*T([0,0,dz])*[crsxval_fnl1(i),crsyval_fnl1(i),crszval_fnl1(i),1]';
    crs_xyplane1 = [crs_xyplane1,r_z0];
end

mm2 = length(crsxval_fnl2);
crs_xyplane2 = [];
for i = 1:mm2
    dz = -crszval_fnl2(i);
    thelta0 = double(dz/k3);
    r_z0 =
Rz(thelta0)*T([0,0,dz])*[crsxval_fnl2(i),crsyval_fnl2(i),crszval_fnl2(i),1]';
    crs_xyplane2 = [crs_xyplane2,r_z0];
end

mm = mm1 + mm2;


%----create points of cross section circle--------
circle = rsmak('circle',R,[0,0]);
```

```
%-------------------------------------

figure,
plot3(crsxval_fnl1,crsyval_fnl1,crszval_fnl1,'b','LineWidth',1.5);
hold on
plot3(crsxval_fnl2,crsyval_fnl2,crszval_fnl2,'r','LineWidth',1.5);
plot(crs_xyplane1(1,:),crs_xyplane1(2,:),'b','LineWidth',2.5);
plot(crs_xyplane2(1,:),crs_xyplane2(2,:),'r','LineWidth',2.5);
fnplt(circle,'c');
plot([0 0],1.2*[-R R]);
plot([-R R]*1.2,[0 0]);

axis equal
title({['Cross section of helical drill at r_i_z=0    '];...
    ['\alpha_y = ',num2str(double(a/pi*180)),'^o  ',...
    '   D_d_r_i_l_l=',num2str(R*2),'mm   D_c_o_r_e=',num2str(R_core*2),'mm'];...
    ['D_w_f_l_u_t_e = ',num2str(R_wheel*2),'mm'];date});
xlabel('X_0');
ylabel('Y_0');
zlabel('Z_0');

hold off
%-----------------------------------------------------------
%the following is to mesh the cylinder and flute sufaces
%-----------------------------------------------------------
x_axis = 0:.5:1;
y_axis = x_axis-x_axis;
z_axis = y_axis;
imax = 31;
jmax =29;
lead = R/tan(1.3109);
alph1 = atan(crs_xyplane2(2,1)/crs_xyplane2(1,1));
alph2 = atan(crs_xyplane2(2,mm2)/crs_xyplane2(1,mm2));
if alph2<0
    alph2 = alph2 + pi;
end

mesh_i_nmbr = mm2;
alph_step = (alph2-alph1)/(mesh_i_nmbr-1);
a_step_cylind = (alph1-alph2+pi)/(mesh_i_nmbr-1);
for i = 1:mesh_i_nmbr
    alph(i) = alph1+(i-1)*alph_step;
    a_cylind(i) = alph2 + (i-1)*a_step_cylind;
    for j = 1:jmax
```

```
        v_v(i,j) = (j-1)/(jmax-1)*double(pi) - .5*double(pi);
        %----------mesh the helix surface, first part------------
        xmesh_0(i,j) =
crs_xyplane2(1,i)*cos(v_v(i,j))-crs_xyplane2(2,i)*sin(v_v(i,j));
        ymesh_0(i,j) =
crs_xyplane2(1,i)*sin(v_v(i,j))+crs_xyplane2(2,i)*cos(v_v(i,j));
        zmesh_0(i,j) = crs_xyplane2(3,i)+double(k3)*double(v_v(i,j));
        %----------mesh the helix surface, second part-----------
        xmesh_1(i,j) = -xmesh_0(i,j);
        ymesh_1(i,j) = -ymesh_0(i,j);
        zmesh_1(i,j) = zmesh_0(i,j);
        %---------------------------------------------------------
        %----------mesh the cylind rical surface----------------
        xmesh_2(i,j) = R*cos(a_cylind(i)+v_v(i,j));
        ymesh_2(i,j) = R*sin(a_cylind(i)+v_v(i,j));
        zmesh_2(i,j) = zmesh_0(i,j);
        xmesh_3(i,j) = -xmesh_2(i,j);
        ymesh_3(i,j) = -ymesh_2(i,j);
        zmesh_3(i,j) = zmesh_0(i,j);
        %---------------------------------------------------------
    end
end

figure, mesh(xmesh_0,ymesh_0,zmesh_0);%helix surface, first part
hold on
plot3(-crsxval_fnl1,-crsyval_fnl1,crszval_fnl1,'b','LineWidth',2.5);
plot3(-crsxval_fnl2,-crsyval_fnl2,crszval_fnl2,'r','LineWidth',2.5);
mesh(xmesh_1,ymesh_1,zmesh_1); %helix surface, second part
mesh(xmesh_2,ymesh_2,zmesh_2); %cylinderical surface
mesh(xmesh_3,ymesh_3,zmesh_3); %cylinderical surface
plotxyzaxes(x_axis,y_axis,z_axis)
axis equal
title({['Efective cutting edge and its corresponding flute    '];...
    ['\alpha_y = ',num2str(double(a/pi*180)),'^o  ',...
    '   D_d_r_i_l_l=',num2str(R*2),'mm   D_c_o_r_e=',num2str(R_core*2),'mm'];...
    ['D_w_f_l_u_t_e = ',num2str(R_wheel*2),'mm'];date});
xlabel('x');
ylabel('y');
zlabel('z');
hold off
```

Appendix B

Code for special functions

1) Function 'Rx'

```
function T=Rx(ax)
%ax=rotating angle about x'
cx=cos(ax);
sx=sin(ax);
max=[1    0      0     0;
    0     cx     -sx   0;
    0     sx     cx    0;
    0     0      0     1];

T=max;
End
```

2) Function 'Ry'

```
function T=Ry(ay)
%ay=rotating angle about y'
cy=cos(ay);
sy=sin(ay);
may=[cy   0      sy    0;
    0     1      0     0;
    -sy   0      cy    0;
    0     0      0     1];

T=may;
end
```

3) Function 'Rz'

```
function T=Rz(az)

cz=cos(az);
sz=sin(az);
maz=[cz  -sz     0    0;
    sz    cz     0    0;
    0     0      1    0;
    0     0      0    1];
```

```
T=maz;
end
```

4) Function 'T'

```
function T=T(translation)

mtrl=[1   0    0    translation(1);
    0    1    0    translation(2);
    0    0    1    translation(3);
    0    0    0    1           ];
T=mtrl;
end
```

5) Function ' findsolution_enhanced '

```
function [a, flag]=findsolution_enhanced(M,V)

digits(30);
dM = diff(M);
x1st = V;
y1st = subs(M,x1st);
tan1st = subs(dM,x1st);
error = double(vpa(abs(y1st)));
error_tan = 10;
i=1;

if tan1st==0
       a = x1st;
       fprintf('failed! curve tangential=%d\n',x1st);
end

while error>0.000000001
    x2nd(1,1)=vpa(x1st-y1st/tan1st);
    x1st(1,1)=vpa(x2nd);
    y1st(1,1)=vpa(subs(M,x2nd));
    tan1st(1,1)=vpa(subs(dM,x2nd));
    error_tan(1,1)=abs(tan1st);
    if error_tan<.00000000001
        fprintf('no solution\n')
        fprintf('endvalue=%d\n',x1st)
        fprintf('interval=%d\n',V)
        a=0;
```

```
        flag = 0;
    end

    error(1,1)=abs(y1st);
    i=i+1;

    if i>40
         fprintf('it is hard to find solution\n')
        fprintf('endvalue=%d\n',x1st)
        fprintf('interval=%d\n',V)
        a = x1st;
        flag = 0;
        return
    end

end
a=x1st;
flag = 1;
return
end
```

6) Function xh_zh_xph_zph_angle

```
function [xh,zh,xph,zph]=xh_zh_xph_zph_angle(h,Rwl_Rcn_W,H)

% % the grinding wheel is a paralle wheel

R_wheel = Rwl_Rcn_W(1);
R1 = Rwl_Rcn_W(2);
R2 = Rwl_Rcn_W(3);
W = Rwl_Rcn_W(4);
W_angle = Rwl_Rcn_W(5);
R = Rwl_Rcn_W(6);

H1 = R_wheel-R1;
H0 = H1-R*1.;
H2 = H1+R1*(double(pi)-W_angle);
H3 = H2+W/sin(W_angle)-R1/tan(W_angle/2)-R2*tan(W_angle/2);
H4 = H3+R2*W_angle;
H5 = H4+R*1.;

syms h real
```

```
if H<0
   display('the value of h should be positive');
   return
end

if H>H5
   display('the value of h is too large');
   return
end

if H<H1&&H>H0
   xh = h;
   zh = 0;
   xph = 1;
   zph = 0;
%    hinterval = [R_wheel-8*R_corner, H1];
else if H<H2
       xh = H1+R1*sin((h-H1)/R1);
       zh = R1-R1*cos((h-H1)/R1);
       xph = diff(xh,'h');
       zph = diff(zh,'h');
%        hinterval = [H1, H2];
   else if H<H3
          xh = H1+R1*sin((H2-H1)/R1)-(h-H2)*cos(W_angle);
          zh = R1-R1*cos((H2-H1)/R1)+(h-H2)*sin(W_angle);
          xph = diff(xh,'h');
          zph = diff(zh,'h');
%           hinterval = [H2, H3];
       else if H<H4
              xh =
H1+R1*sin((H2-H1)/R1)-(H3-H2)*cos(W_angle)-R2*sin(W_angle)+R2*sin(W_angle-(h-H3)/R2
);
              zh =
R1-R1*cos((H2-H1)/R1)+(H3-H2)*sin(W_angle)-R2*cos(W_angle)+R2*cos(W_angle-(h-H3)/R2
);
              xph = diff(xh);
              zph = diff(zh);
%               hinterval = [H3, H4];
          else if H<H5
                 xh = 2*H4-h;
                 zh = W;
                 xph = -1;
                 zph = 0;
%                  hinterval = [H4, H4+H5];
```

```
            end
        end
    end
end
end

% H12345 = [H1 H2 H3 H4 H5];
```